The Astronomical Journal, 123:2417–2437, 2002 May

THE VLA H I OBSERVATIONS OF STEPHAN'S QUINTET (HCG 92)[1]

B. A. Williams
Department of Physics and Astronomy, University of Delaware, Newark, DE 19716; baw@udel.edu

Min S. Yun
Department of Astronomy, University of Massachusetts, Amherst, MA 01003; myun@astro.umass.edu

and

L. Verdes-Montenegro
Instituto de Astrofísica de Andalucía, CSIC, Apdo. Correos 3004, E-18080 Granada, Spain; lourdes@iaa.es
Received 2001 December 28; accepted 2001 January 24

ABSTRACT

Using the Very Large Array, we have made spectral-line and continuum observations of the neutral hydrogen in the direction of the compact group of galaxies Stephan's Quintet. The high-velocity clouds between 5600 and 6600 km s^{-1}, the disk of the foreground galaxy NGC 7320 at 800 km s^{-1}, the extended continuum ridge near the center of the group, and three faint dwarflike galaxies in the surrounding field were imaged with the C, CS, and D configurations. Four of the H I clouds previously detected are confirmed. The two largest H I features are coincident with and concentrated mainly along separate large tidal tails that extend eastward. The most diffuse of the four clouds is resolved into two clumps, one coinciding with tidal features south of NGC 7318A and the other devoid of any detectable stellar or Hα sources. The two compact clouds along the same line of sight have peak emission at luminous infrared and bright Hα sources probably indicative of star-forming activity. The total amount of H I detected at high redshifts is $\sim 10^{10} M_{\odot}$. As in previous H I studies of the group, no detectable emission was measured at the positions of any high-redshift galaxies, so that any H I still bound to their disks must be less than $2.4 \times 10^7 M_{\odot}$.

Key words: galaxies: clusters: general — galaxies: clusters: individual (HCG 92, Stephan's Quintet) — galaxies: evolution — galaxies: interactions — ISM: atoms

1. INTRODUCTION

Stephan's Quintet (SQ, Arp 319) was the first compact group to be discovered in the late 1800s, and it is probably the best-known and most-studied dense group at all wavelengths. The original membership identified by Stephan (1877) included five bright, relatively isolated galaxies (NGC 7317, 7318A/B, 7319, and 7320) in a tight configuration on the sky. In addition to their close proximity, three of the spiral members (NGC 7318A/B, 7319) have peculiar or highly distorted optical images that include faint wisps, filaments, and tails. Given its high surface brightness (22.3 mag $arcsec^{-2}$, Hickson 1982) and surface density enhancement (593, Sulentic 1987), it is no surprise to find the quintet included among the Hickson groups (Hickson 1982, 1993). While the physical compactness of most HCGs has been challenged (see Barnes 1996 and references therein), the optical evidence of recent tidal interactions leaves little doubt that some of the galaxies in the quintet are physically close. As is typical of Hickson groups (Sulentic 1997), the quintet contains a discordant-redshift member (NGC 7320). A difference in redshift of nearly 6000 km s^{-1} between NGC 7320 and the high-redshift members was first reported by Burbidge & Burbidge (1961), who concluded that NGC 7320 is either a member of the dense group or a foreground galaxy. The discovery of the discordant redshift in SQ and similar groups such as Seyfert's Sextet and VV 172 (Vorontsov-Velyaminov 1959) sparked much debate concerning the relationship between the high- and low-redshift galaxies in compact configurations and noncosmological redshifts.

Initially, 21 cm line studies of SQ were undertaken mainly with the hope that the radio observations would provide distances independent of redshift, thereby resolving both questions about the group's membership and the existence of noncosmological redshifts. Allen (1970) was the first to detect H I emission in the direction of the quintet. This emission, detected at 800 km s^{-1}, was associated with NGC 7320. Using the integral properties derived from the H I profile and comparing them with similar properties of field galaxies, Allen (1970) concluded that NGC 7320 is a dwarf galaxy at a distance consistent with its redshift. Because Allen's study did not resolve the question of group membership, Balkowski et al. (1973) and Shostak (1974) were motivated to search for H I emission from other quintet galaxies that possibly could. Both detected H I emission near 6600 km s^{-1}, which they attributed to NGC 7319. After applying the same method used by Allen (1970), they derived very different distances. Balkowski et al. (1973) placed the galaxy at the same distance as NGC 7320, while Shostak (1974) found it more likely that NGC 7319 belongs at a distance commensurate with its redshift. The difference in their distances can be traced to the calibration samples that each adopted. The main weakness of this method used to derive distances was the underlying assumption that the galaxies in the quintet have normal H I properties for their morphological types and luminosity. Using the Westerbork Synthesis Radio Telescope (WSRT), Allen & Sullivan (1980) would test this assumption by providing new information on the distribution and kinematics of the H I gas in the quintet. Their observations supported the assumption of normalcy in the

[1] The National Radio Astronomy Observatory is a facility of the National Science Foundation operated under cooperative agreement by Associated Universities, Inc.

location and motion of the low-redshift H I but raised serious doubt about the use of H I profiles as distance indicators when the data showed the gas at 6600 km s^{-1} in an extended cloud ($2\farcm5 \times 4'$) not directly associated with any of the members.

The discovery of an isolated cloud in SQ was significant because it alone changed the focus of subsequent 21 cm line studies. H I observations more sensitive to extended emission over larger regions of the quintet were undertaken in an effort to understand this anomalous feature in the context of the group's origin and evolution. Sensitive H I searches using the Arecibo telescope found the presence of low-level (8 mJy) broadband emission between 5600 and 6600 km s^{-1} (Sullivan 1980) and two more features extended and offset from the quintet galaxies (Peterson & Shostak 1980). With better angular resolution and sensitivity than the old observations (Allen & Sullivan 1980), Shostak et al. (1984) used the WRST to locate and confirm the three cloud features at 5700, 6000, and 6600 km s^{-1} that had been previously detected. Their synthesis observations showed the H I largely outside the optical boundaries of the galaxies in the quintet.

This present study of SQ is part of a broader investigation of the distribution and kinematics of H I in the least and most compact associations in the Hickson catalog (Williams et al. 1999a, 1999b; Verdes-Montenegro et al. 2000a, 2000b, 2001; Huchtmeier et al. 2000) in order to analyze the type and effect of the interactions that are taking place. If physically dense, Hickson groups are natural sites for studying tidal interactions and their effects, galaxy formation and evolution via merging processes, and the dynamical evolution of galaxy groups. Spiral galaxies normally more extended in H I than in starlight are susceptible to tides and direct collisions and ought to be more sensitive to recent interactions. High-resolution imaging of the neutral hydrogen can be used to distinguish between the real and illusory compact groups and may provide a sensitive test of the dynamical evolution of the physically dense groups. We have analyzed the spatial distributions and kinematics of H I within a subset of 16 groups and proposed an evolutionary scenario where the amount of detected H I would decrease further with evolution, either by continuous tidal stripping and heating or by shocks produced when galaxies penetrate the group's core and interact violently with the interstellar or intergalactic H I in the groups (Verdes-Montenegro et al. 2001). SQ, among the densest Hickson groups, is a vital constituent in this scenario; hence its detailed study would be essential in characterizing the extreme stages in galaxy interactions and group evolution.

There is strong observational evidence that SQ is a physical system. The filaments, tails, and peculiar images of the galaxies are suggestive of interactions. The distribution of the H I outside the galaxies is consistent with a history of collisional encounters that may have stripped the spiral members of their H I disks (Allen & Sullivan 1980; Shostak et al. 1984). Why then observe SQ with the Very Large Array (VLA)? What more had we hoped to learn from H I synthesis observations? The WRST (Shostak et al. 1984) integrated map gives us a clear sense of how the gas between 5700 and 6600 km s^{-1} is distributed. Given the higher angular and velocity resolution of the VLA, we saw an opportunity to improve the kinematical description of the H I gas already detected outside of the galaxies. With its higher sensitivity to faint compact emission, the VLA could detect additional isolated H I clouds within the quintet and possibly resolve any weak H I emission associated with tidal features or still bound to the disks of the individual galaxies.

2. OBSERVATIONS AND DATA REDUCTION

Observations of SQ were first made with the VLA in its 3 km (C) configuration on 1991 January 1, using all 27 telescopes. The observational parameters are summarized in Table 1. Additional observations of HCG 92A (centered at 782 km s^{-1}) and the emission at 5700 km s^{-1} missed in the original observations were made in the CS configuration, which includes the 3 km baselines and some extra short spacings (Rupen 1999). To improve sensitivity to extended, low surface brightness sensitivity, additional D-configuration data were obtained in 1999 March 28. Shortest baselines at the shadowing limit of 25 m are present, and structures as large as $15'$ in size should be visible in each channel map. All of the data are calibrated following the standard VLA calibration procedure in AIPS and imaged using IMAGR. Absolute uncertainty in the resulting flux scaling is about 15%, and this is the formal uncertainty we quote for all physical parameters derived from the flux density. The synthesized beam, produced using a robust weight of $R = 0.5$, is $19\farcs4 \times 18\farcs6$. The resulting spectral-line maps have a velocity resolution of 21.5 km s^{-1} and an rms noise level of 0.21 mJy (0.38 K). The 3 σ H I flux limit in each map is about 0.015 Jy km s^{-1}, corresponding to an H I column density limit of 5×10^{19} atoms cm^{-2}. At the adopted distance of the compact group (85 Mpc) and at the distance of HCG 92A (10 Mpc) the mass detection limit is 2.4×10^7 $M_\odot$ and 3.5×10^5 $M_\odot$, respectively.[2]

[2] The atomic gas mass has been calculated as $M_{\rm H\,I} = 2.36 \times 10^5\ D^2_{\rm Mpc} \int S_v dv$, where $S_v dv$ is in Jy km s^{-1}.

TABLE 1
SUMMARY OF OBSERVATIONS

Parameter	rms Noise (mJy beam^{-1})	rms Noise (K)	Channel Width (km s^{-1})	Velocity Range (km s^{-1})	Beam Size (arcsec)
Natural Weighting:					
H92a	0.20	0.34	20.7	475–1097	19.4 × 18.6
IF1	0.21	0.38	21.5	6272–6918	19.4 × 18.6
IF2	0.21	0.38	21.5	5725–6326	19.4 × 18.6

3. CONTINUUM EMISSION

A line-free continuum image constructed by averaging the 21 line-free channels is shown in Figure 1, and the main parameters of the emission are given in Table 2. This 15″ resolution image has an effective bandwidth of 2.05 MHz centered on an effective frequency of 1416 MHz. The rms noise level achieved in Figure 1 is 0.10 mJy beam^{-1} (0.3 K). This continuum image is a factor of 3 more sensitive in flux density and about 30 times more sensitive in surface brightness than the best continuum map produced by van der Hulst & Rots (1981).

In its gross details our continuum map is in good agreement with the 6″ resolution image generated by van der Hulst & Rots (1981) and with other published continuum maps (Allen & Hartsuiker 1972; Shostak et al. 1984). Besides detecting the two unresolved northern sources and the extended linear source between NGC 7318B and NGC 7319, an unresolved continuum source coincident with the nucleus of NGC 7318A is also clearly detected. A possible detection of a source associated with the nucleus of NGC 7320 is also made (Fig. 1). More importantly, the new continuum image delineates the diffuse emission more clearly than ever before.

The bright radio nucleus of NGC 7319 has a flux density of 27 ± 4 mJy, in good agreement with the results of van der Hulst & Rots (1981) and Allen & Hartsuiker (1972). Their high-resolution VLA data show a short (6″) jetlike feature emanating southwestward from the nuclear source in NGC 7319 (see Fig. 3 of van der Hulst & Rots 1981). The other unresolved source to the northwest has no optical counterpart brighter than 29 mag arcsec^{-2} (see Fig. 10, Arp 1973), and it may be an unrelated background source. Its flux density is 10 ± 1 mJy. The radio source coincident with the nucleus of NGC 7318a was only marginally detected (at the 3 σ level) by van der Hulst & Rots (1981). We confirm their detection of the nuclear radio source in NGC 7318A and find that its flux density is 1.4 ± 0.2 mJy, consistent with their measurement. The new continuum image (Fig. 1) also shows a 3.6 σ source nearly coincident with the nucleus of NGC 7320.

The high surface brightness sensitivity achieved by the new observations reveals for the first time the faint structure in the extended radio ridge between NGC 7318B and NGC 7319. The new continuum image shows the smooth connection of the entire north-south ridge, from the bright northern unresolved source to the elongated north-south feature

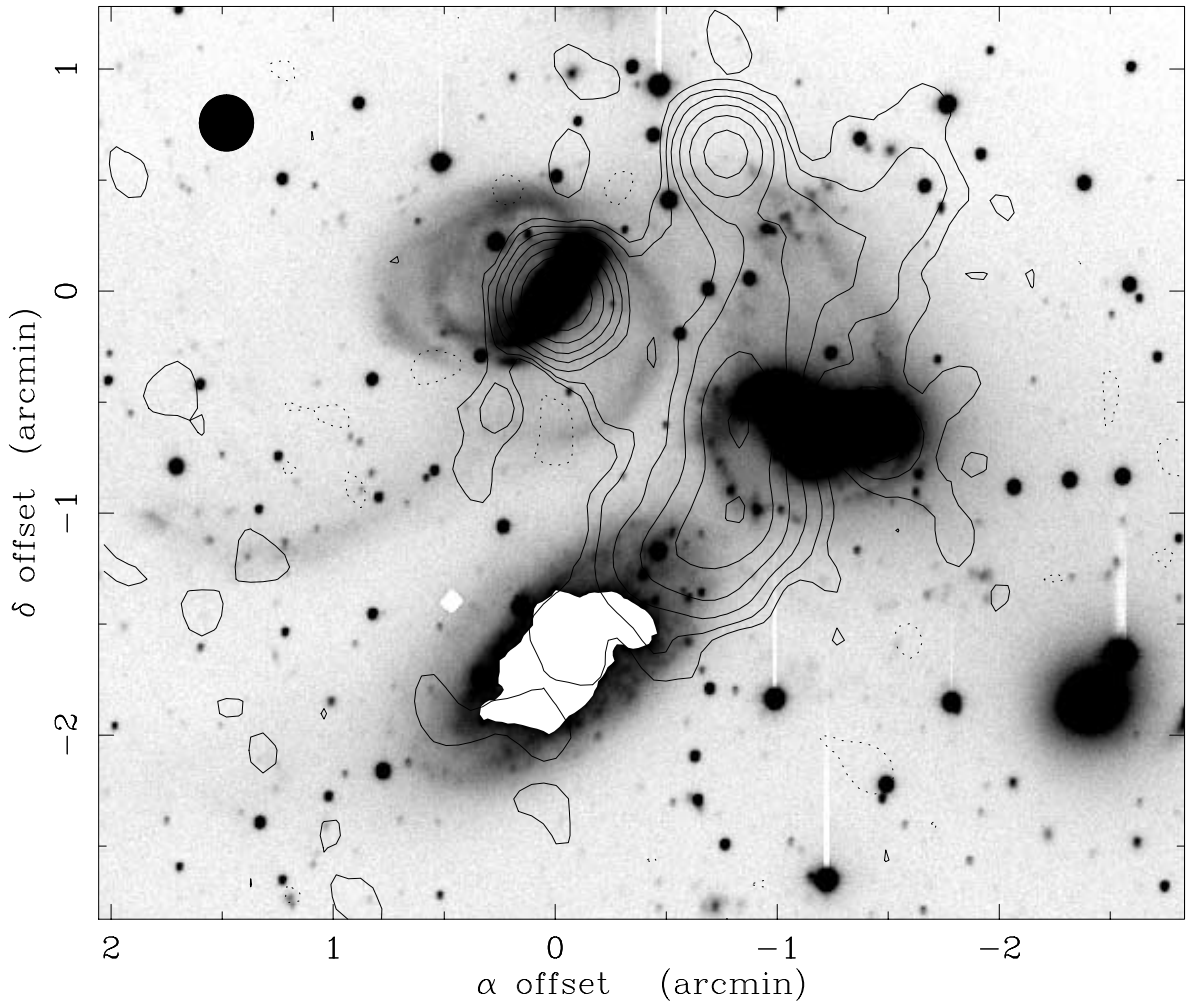

FIG. 1.—Contour map of the 21 cm continuum emission in HCG 92 overlaid on an *R*-band image obtained by J. Sulentic at the 3.5 m CAHA telescope. The contours are −0.2, 0.2, 0.4, 0.8, 1.6, 3.2, 6.4, 13, and 26 mJy beam^{-1}. The synthesized beam, 15″.4 × 14″.8, is shown on the upper left corner. Coordinate offsets are with respect to the optical nucleus of NGC 7319 at $\alpha_{B1950.0} = 22^h33^m46^s1$, $\delta_{B1950.0} = 33°43'00''$.

TABLE 2
1.4 GHz Continuum Emission in HCG 92

Name	Size	Flux (mJy)	$L_{1.4\,\mathrm{GHz}}$ (W Hz^{-1})
NGC 7317.....	...	<0.3	$<2.3 \times 10^{17}$
NGC 7318A.....	<5″	1.4 ± 0.2	$(1.1 \pm 0.2) \times 10^{18}$
NGC 7318B	...	...	...
NGC 7319.....	<5″	27 ± 4	$(2.1 \pm 0.3) \times 10^{19}$
NGC 7320.....	<5″	0.4 ± 0.1	$(4.8 \pm 1.2) \times 10^{15}$
NGC 7320C	<5″	<0.3	$<2.3 \times 10^{17}$
Radio core	<5″	10 ± 1	$(7.5 \pm 1.1) \times 10^{18}$[a]
Radio filament	0.′5 × 2.′5	48 ± 7	$(3.6 \pm 0.5) \times 10^{19}$
Total	...	96 ± 15	...

[a] Assuming a distance of 85 Mpc, the same as for SQ.

1.′5 to the south. An eastern extension connecting to the nucleus of NGC 7319 and a northwestern extension coincident with the string of Hα emission (Plana et al. 1999; Sulentic et al. 2001) north of NGC 7318B are present in the faint radio emission. The total flux density associated with the extended radio ridge is 48 ± 7 mJy, which is at least 60% smaller than that measured by van der Hulst & Rots (1981). The brightness distribution and the extent of the radio ridge closely follow the extended X-ray emission imaged with *ROSAT* (Sulentic et al. 1995; Pietsch et al. 1997) and the extended Hα emission (Ohyama et al. 1998; Xu et al. 1999). By itself the radio continuum emission in the direction of the quintet might be interpreted as a chance superposition of a background core-jet source unrelated to the group; however, the spatial coincidence of the radio ridge, Hα emission, and X-ray emission would be unusual, and it would be difficult to explain in radio plumes and rarely detected in radio core-jet sources. Furthermore, the radio continuum emission is less likely to be a random background source since its east-west extension also coincides with Hα emission at the same mean velocity as the H I gas in the group.

4. HCG 92A (NGC 7320)

The new VLA H I image of NGC 7320 shown in Figure 2*a* reveals an unperturbed normal H I disk with a small central depression surrounded by an H I ring or a pair of tightly wound spiral arms. The total extent of the H I disk is 2.′5 × 1.′5 (7.3 kpc × 4.4 kpc at $D = 10$ Mpc), comparable in size to the optical image. We plot in the upper left corner of Figure 2*a* the integrated profile obtained by integrating the flux density in each channel map. The total H I flux, $\int S_v dv$, recovered by the VLA is 8.25 ± 0.05 Jy km s^{-1}, corresponding to an H I mass $M_{\mathrm{H\,I}} = 1.95 \pm 0.01 \times 10^8\ M_\odot$. Although our sensitivity is sufficient to detect clouds with an H I mass of at least $3.5 \times 10^5\ M_\odot$, no other H I sources within the 15′ (45 kpc) radius region mapped at frequencies near 1417 MHz were detected. The H I properties of NGC 7320 are listed in Table 3.

The apparent blue magnitude of NGC 7320 is listed as 13.23 mag by de Vaucouleurs et al. (1991, hereafter RC3). Corrections for internal extinction (Sandage & Tammann 1981), for Galactic extinction as determined Fisher & Tully (1981b), who adapted from Burstein & Heiles (1978), and for the effect of redshift are 0.53, 0.39, and 0.075 mag, respectively. Application of the three corrections above yields a blue absolute luminosity $L_B = 2.0 \times 10^9\ L_\odot$ for this small, Sd galaxy. Its $M_{\mathrm{H\,I}}/L_B$, a measure of the H I gas content in solar units, is only 0.10 and is more characteristic of the H I content associated with early-type spiral galaxies. We derive an H I surface density $\sigma_{\mathrm{H\,I}} = M_{\mathrm{H\,I}}/0.25\pi a_0^2 = 8.0 \pm 10^{-4}$ g cm^{-2} $= 3.8\ M_\odot$ pc^{-2}, where a_0 is the corrected isophotal major diameter taken from RC3. This value is abnormally low when compared with the average H I surface density of Sd galaxies in a sample of nearby galaxies (Huchtmeier & Richter 1988) and in the larger sample of Roberts & Haynes (1994). The total H I mass we derive is in good agreement with the previous measurements (Allen 1970; Gordon & Gordon 1979; Allen & Sullivan 1980; Sulentic & Arp 1983), and this low $M_{\mathrm{H\,I}}/L_B$ ratio is not the result of H I missed by the VLA observations.

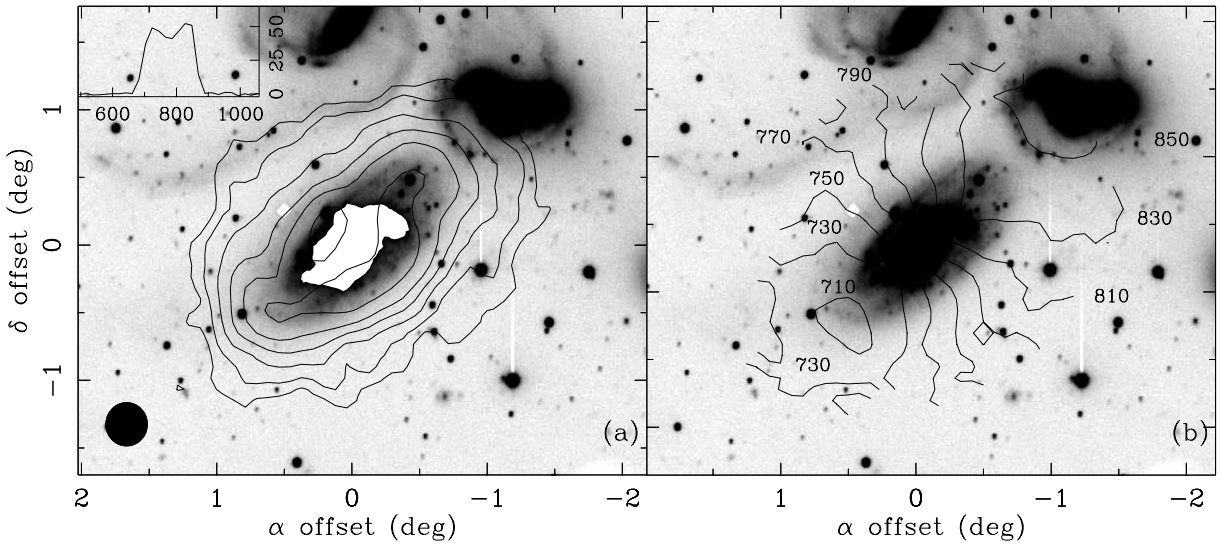

Fig. 2.—(*a*) Map of the H I column density distribution in HCG 92A superposed on the same *R* image shown in Fig. 1. The contours are 9, 18, 36, 60, 89, and 134 × 10^{19} atoms cm^{-2} and the beam size 19.″4 × 18.″6. The H I flux density in millijanskys is plotted as a function of heliocentric velocity in kilometers per second in the upper left corner. (*b*) Map of the first-order moment of the radial velocity field. The numbers indicate heliocentric velocities in kilometers per second.

TABLE 3
SUMMARY OF H I OBSERVATIONS OF HCG 92A[a]

Parameter	HCG 92A
$\langle V_{\rm H\,I}\rangle$ (km s^{-1})	776 ± 10
Velocity width (km s^{-1})	192 ± 10
Size (arcmin)	2.5 × 1.5
Size (kpc)	7.3 × 4.4
Peak flux (Jy km s^{-1})	0.55 ± 0.01
Peak $N_{\rm H\,I}$ (10^{21} cm^{-2})	1.65 ± 0.03
Peak A_V (mag)	0.77
Integrated flux (Jy km s^{-1}):	
Shostak et al. 1984	7.8
New VLA	8.25 ± 0.05
$M_{\rm H\,I}$ (10^9 $M_\odot$)	0.195 ± 0.001

[a] Assuming distance of 10 Mpc for HCG 92A.

The observed H I kinematics (Figs. 2*b* and 3) is that of normal disk rotation, without any signs of tidal distortions. The derived rotation curve, shown in Figure 4, gradually rises out to a radius of 60″ (3 kpc), where it peaks at a value of 95 ± 3 km s^{-1}. Both fits to the H I image and kinematics give a position for the galaxy's center at $\alpha_{1950.0} = 22^{\rm h}33^{\rm m}45\overset{\rm s}{.}8$, $\delta_{1950.0} = 33^\circ41'21\overset{''}{.}5$, a position angle of $-51^\circ \pm 1^\circ$ for the major axis, and a disk inclination of $i = 48^\circ \pm 2^\circ$. We find that the H I isophotal and dynamical centroids agree within a few arcseconds of each other; therefore, previous reports of a displacement by Allen & Sullivan (1980) and Sulentic & Arp (1983) are not supported by the new data.

Using the best-fitting parameters to the derived rotation curve in Figure 4, we estimate a total mass $M_T = (3/2)^{3/n} D V_{\rm max}^2 R_{\rm max}/G = 2.2 \times 10^{10}\ M_\odot$, based on Brandt (1960) parametrization of the rotation curve, where $V_{\rm max}$ is the maximum rotational velocity, $R_{\rm max}$ is the radius at which this velocity first occurs, and n is a parameter that

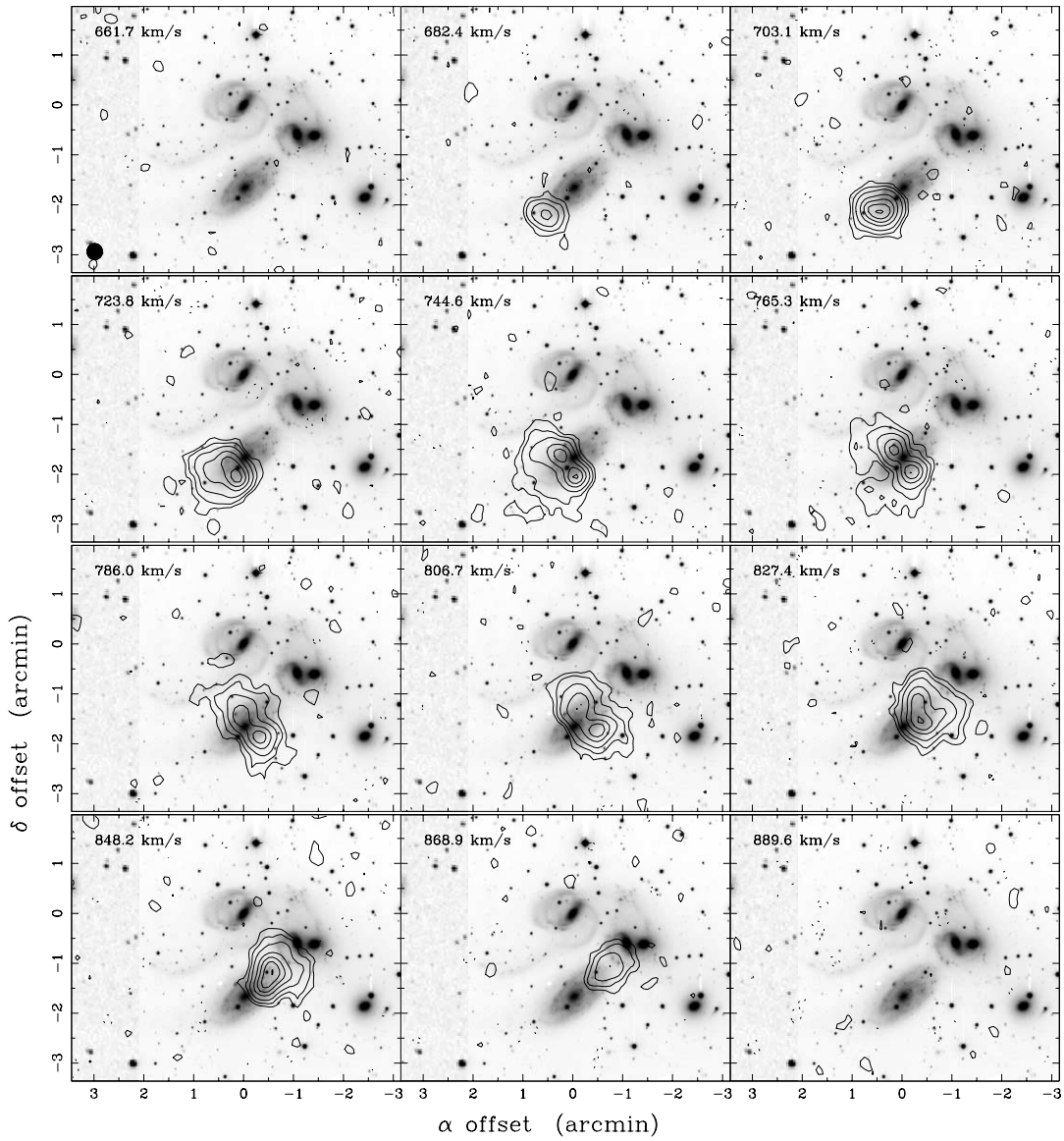

FIG. 3.—Channel maps of the 21 cm line radiation of HCG 92A superposed on the same *R* image as in Fig. 1. The Palomar Observatory Sky Survey (POSS) image has been used for the eastern part of the field. The contours are −1.6, 1.6, 3.2, 6.6, 13, 20, 26, 33 × 10^{18} atoms cm^{-2}.

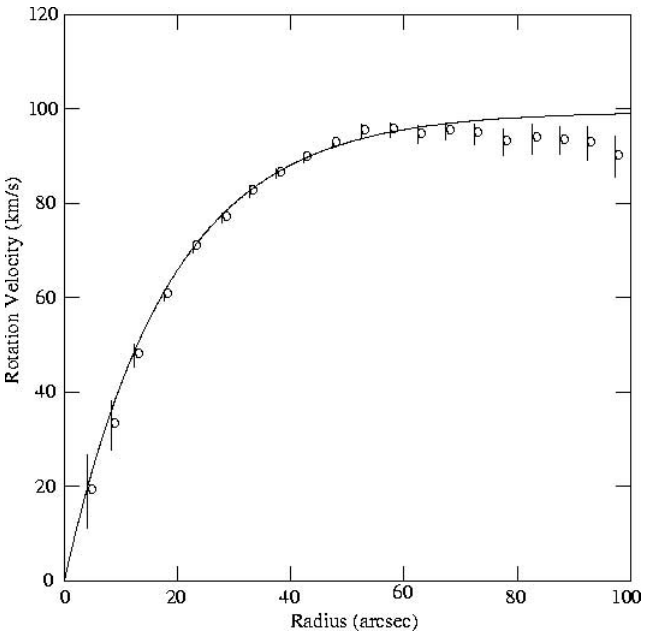

FIG. 4.—Rotation curve for NGC 7320 derived from the intensity weighted mean velocity map (Fig. 2*b*). The solid line represents an exponential rotation curve of the form $V_{\rm rot}/V_{\rm max} = 1 - e^{-R/R_{\rm max}}$. The best-fit parameters are $V_{\rm max} = 99$ km s^{-1} and $R_{\rm max} = 85''$.

describes the shape of the derived rotation curve beyond $R_{\rm max}$. We assumed in the calculation of total mass above that $n = 1.3$, which corresponds to a flat curve beyond $85''$. With the values of M_T, $M_{\rm HI}$, and L_B given, we obtain for the integral properties of NGC 7320 $M_T/L_B = 11$ in solar units and $M_{\rm HI}/M_T = 0.01$. The value of M_T/L_B is reasonable for its morphological type, but the ratio $M_{\rm HI}/M_T$ is low (Roberts & Haynes 1994). It is clearly the H I integrated properties of NGC 7320 that are peculiar, and not its kinematics.

Materne & Tammann (1974) were the first to provide evidence that NGC 7320 is probably a member of the stable group that includes the supergiant galaxy NGC 7331. Projected less than 100 kpc away from the center of this galaxy, NGC 7320 is probably a companion to (if not a satellite of) this prominent spiral (Tammann 1970). The low H I integrated properties measured for the dwarf galaxy are more likely related to interactions with the halo of NGC 7331, rather than interactions among the high-redshift members of SQ. In summary, our new H I observations firmly establish that NGC 7320 is a relatively unperturbed, foreground galaxy projected against the high-redshift members of the quintet.

5. THE QUARTET REGION

If our assumption about the distance of NGC 7320 is correct, then the other four galaxies, NGC 7317, 7318A/B, and 7319, form a bright *quartet* at an adopted distance of 85 Mpc. Assuming a constant mass-to-light ratio of $M_{\rm tot}/L_B = 7$ in solar units, we derived this distance from a recessional motion of 6480 km s^{-1} (corrected for Galactic rotation and Virgocentric flow) for the quartet's center of mass and a Hubble constant $H_0 = 75$ km s^{-1} Mpc^{-1}. The neutral hydrogen is detected between 5597 and 6755 km s^{-1}, well displaced from the positions of the high-redshift galaxies (Fig. 5), a result first reported by Allen & Sullivan (1980) and later confirmed in greater detail by Shostak et al. (1984). The redshift range would place the gas at the same distance as the quartet's center of mass. No emission brighter than 0.4 mJy beam^{-1} is detected at the positions of any high-redshift galaxies in the quintet including NGC 7320C, a likely fifth member located $3'$ east of NGC 7319. The H I emission concentrates in three discrete velocity bands: 6475–6755 km s^{-1}, 5939–6068 km s^{-1}, and 5597–5789 km s^{-1}. It is mostly contained within five physically distinct components: a large curved feature composed of two arclike clouds (Arc-S and Arc-N) just east of the quartet and west of NGC 7320C, two kinematically distinct clouds (NW-LV, NW-HV) projected along the same direction north of NGC 7318A/B, and one diffuse feature (SW) between NGC 7318A/B and NGC 7317.

5.1. *Distribution and Kinematics of the* H I *Gas*

5.1.1. *Arc Feature: Large Tidal Tail(s)?*

The bulk of the H I (58%) is detected in the large L-shaped arc feature located about $3'$ (75 kpc) southeast of the quartet's center (see Fig. 5). It extends over $5'$ in size and has a mean radial velocity of 6610 km s^{-1}, which is about 130 km s^{-1} redshifted with respect to the group's center of mass. This feature gives an impression of being a single long structure (>125 kpc), possibly of tidal origin, but a careful examination of its morphology, kinematics, and velocity dispersion suggests two distinct features. The clear morphological evidence for two separate features is the two parallel tidal tails visible on the northeastern side of NGC 7319 in deep optical images (see our Fig. 5 and also Fig. 8 of Arp & Lorre 1976).

The northern part of the H I cloud (Arc-N; Fig. 6*a*) traces the optical tail emerging eastward from NGC 7319 toward NGC 7320C. The curvature of the H I contours matches that of the bright optical tidal tail. Peak emission where the column density reaches 10^{21} atoms cm^{-2} ($\alpha_{1950.0} = 338\overset{\circ}{.}47$, $\delta_{1950.0} = 33\overset{\circ}{.}70$) is coincident with a 15 μm star-forming region (source B of Xu et al. 1999) and a luminous Hα emission object (source C1 of Arp 1973). The line width associated with this region is larger than 100 km s^{-1}, substantially larger than other parts where the line width is barely resolved by the 21.5 km s^{-1} channels (Fig. 7). Faint emission associated with this feature continues to extend $2'$ (50 kpc) northward (Fig. 6*a*) into the region between NGC 7319 and NGC 7320C, where Shostak et al. (1984) also detected extended H I at $\alpha_{1950.0} = 338\overset{\circ}{.}46$, $\delta_{1950.0} = 33\overset{\circ}{.}73$.

The southern part of this cloud (Arc-S; Fig. 6*b*) is coincident with the fainter, less prominent optical tail passing behind NGC 7320 and curving well beyond its southern tip. Emission associated with this feature is diffuse and ends sharply in the northwest, where the continuum ridge begins. The H I emission peak in the southern tail is coincident with the Hα regions A12 and A14 in Arp (1973), while the H I peak at the southern tip of NGC 7320 includes the Hα sources A1, A2, A3, and A4 (Arp 1973).

Comparisons between the WSRT and VLA maps in the direction of NGC 7320 are severely limited by the lack of WSRT data across a third of the galaxy's disk (see Fig. 3 of Shostak et al. 1984). We do not detect any emission brighter than 0.44 (2 σ) mJy beam^{-1} in the region just south of NGC 7319 and east of NGC 7318B (Fig. 8). Yet, the WSRT integrated map in this direction (Fig. 3 of Shostak et al. 1984) clearly reveals an extended condensation having a H I col-

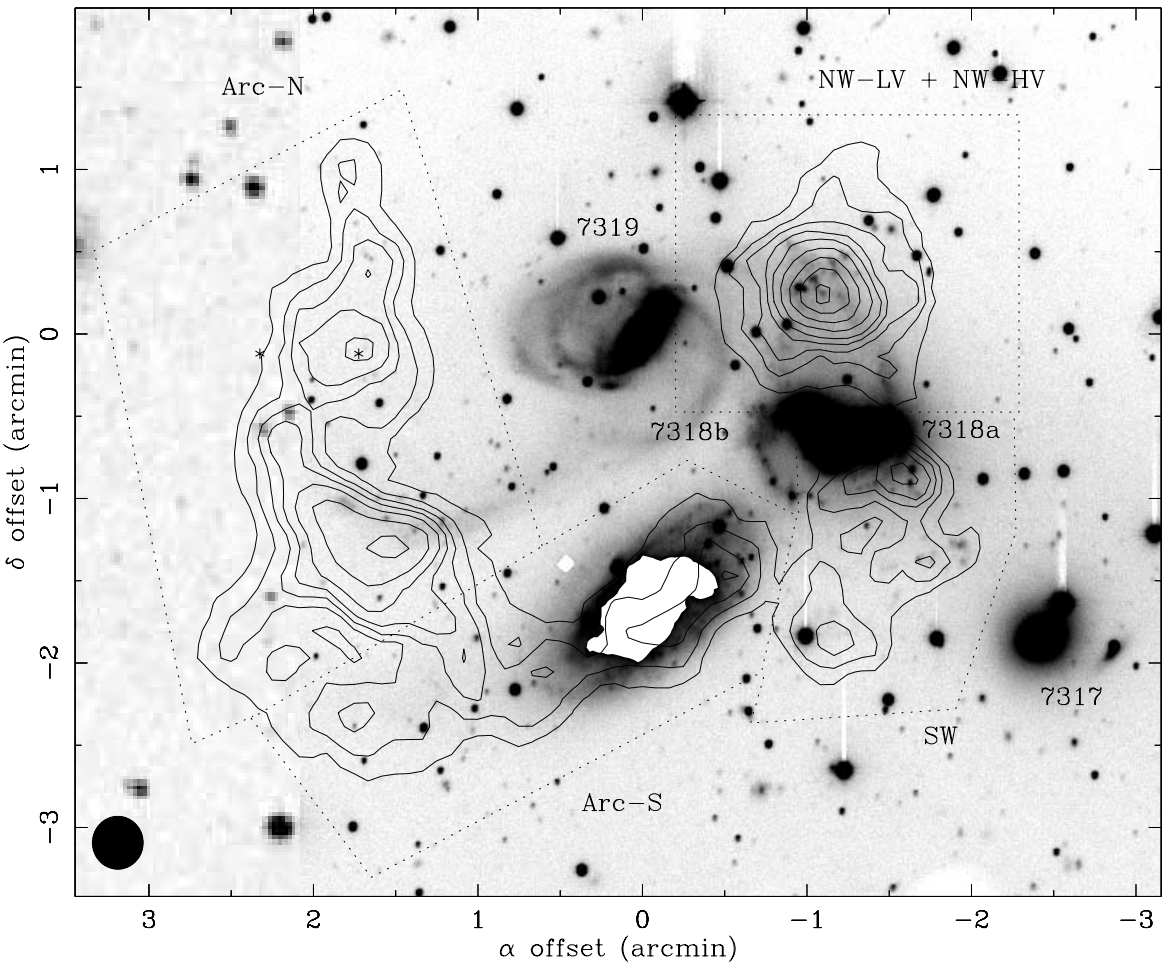

FIG. 5.—Map of the total H I column density distribution in HCG 92 superposed on the same *R* image as in Fig. 1. The POSS image has been used for the eastern part of the field. The integration range is from 5597 to 6918 km s^{-1} and the contours are 5.8, 15, 23, 32, 44, 61, 87, 120, 180 $\times$ 10^{19} atoms cm^{-2}. The synthesized beam is 19.″4 $\times$ 18.″6.

umn density between (1–4) $\times$ 10^{20} atoms cm^{-2}. Even though this reported surface brightness is well above the VLA sensitivity limit (see § 5.2), it was not imaged in our VLA map, nor in Fig. 6 of Allen & Sullivan (1980). As we discuss in § 5.2, we suspect that the difference is related to the effect of residual radar interference and unstable levels in the continuum emission that compromised the quality of the WSRT data.

The intensity-weighted mean velocity map (Fig. 8*b*) shows nearly constant line-of-sight velocity along the entire length of Arc-N. In contrast, the velocity gradient observed along Arc-S is monotonic and nearly linear, characteristic of a streaming motion typically associated with tidal tails (e.g., Hibbard & Mihos 1995). The radial velocity increases by 100 km s^{-1} over an angular distance of 2.′5 (62 kpc) in a northwestern direction across this fainter tail. Shostak et al. (1984) did not detect this feature; instead, they report a similar velocity gradient across Arc-N that the VLA does not confirm.

All of the Hα regions cited above have been cataloged by Arp (1973) as high-redshift objects, i.e., optical sources with radial velocities between 5700 and 6700 km s^{-1}. C1 has a redshift greater than 6500 km s^{-1}. The ionized gas has radial motions consistent with that of the H I gas detected in the directions of both optical tidal tails. Moles et al. (1998) found no evidence of low-redshift Hα sources in the southern optical tail and concluded that it is a background feature to NGC 7320. Our H I data confirm this finding. The similarity between the shape of the H I emission and the optical tails and the spatial correlation between the H I emission peaks and high-redshift Hα regions would indicate that the gas in the tidal tails is associated with the quartet rather than with the disk of NGC 7320.

5.1.2. *NW Features*

H I emission north of NGC 7318 is detected in two compact clouds at two *distinct* velocities, projected along the same direction at $\alpha_{1950.0} = -1.'2$, $\delta_{1950.0} = 0.'25$, near the crossing point of the two tidal features (Figs. 8 and 9) north of NGC 7318A/B. In the intermediate-frequency (IF) band centered at 1389.9 MHz (6595 km s^{-1}), emission around this position is present in 12 velocity channels (Fig. 7) and contained within a slightly resolved feature, NW-HV (Fig. 9*b*). This feature was first discovered with WSRT by Shostak et al. (1984). It shows a large velocity gradient along a position angle of $\sim$50°, with the mean radial velocity increasing 60 km s^{-1} to the SW over an angular distance of 0.′7 or 17.3 kpc (Fig. 8*b*). In the higher IF band centered at 1392.5 MHz (6025 km

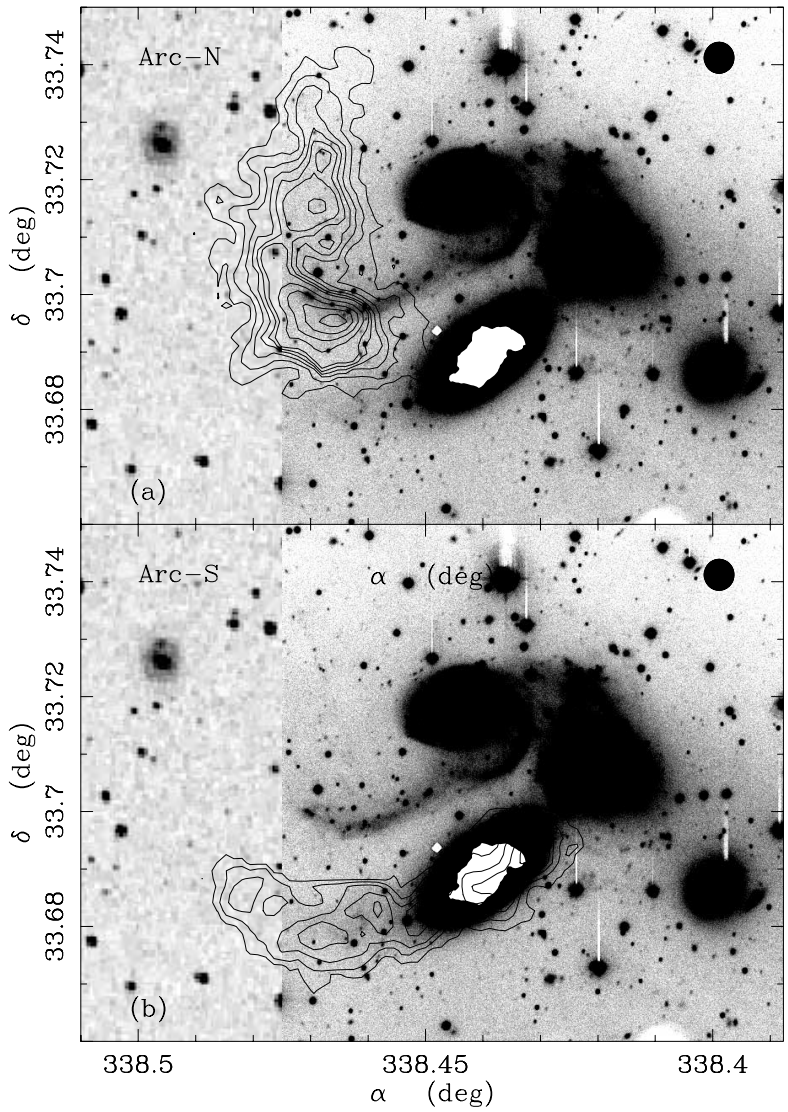

FIG. 6.—Map of the H I column density distribution in HCG 92 Arc-N (*a*) and Arc-S (*b*) superposed in the same *R* image shown in Fig. 1. The POSS image has been used for the eastern part of the field. The contours are 1.5, 5.8, 12, 18, 23, 29, 44, 58, 73, and 87 × 10^{19} atoms cm^{-2} and the synthesized beam is 19″.4 × 18″.6.

s^{-1}), H I is present in seven velocity channels (Fig. 10) and is confined to the more extended cloud feature NW-LV. This low-velocity cloud was also originally detected in the WSRT data and was dubbed "West A" by Shostak et al. (1984). Its velocity gradient is similar in magnitude, but nearly opposite in direction, to that of NW-HV, along a position angle of 40°, over an angular distance of 1′ or 25 kpc (Fig. 9*b*).

Detailed examinations of the channel maps in Figs. 7 and 10 reveal clear differences between the two NW features in that the NW-LV feature is much more extended spatially (>30 kpc), following along both optical tidal features, while the NW-HV feature is far more compact. The H I emission peaks in NW-HV and NW-LV are coincident at the resolution of these observations and lie in the same direction as the luminous 15 μm source A of Xu et al. (1999) and several bright Hα sources that are probably indicative of star-forming activity embedded in the densest regions of the gas. B10, a luminous Hα source cataloged by Arp (1973), sits near this H I peak. Moles et al. (1998) identify this same Hα source as K3 and report a radial velocity of 6680 km s^{-1}, in good agreement with that reported by Plana et al. (1999) for their source 6 (6670 km s^{-1}), and this Hα source is associated with the NW-HV feature. On the other hand, B11 and B13 (Arp 1973), other Hα sources that align with the H I peak, appear to be related to the NW-LV feature. These Hα sources, later renamed K1 and K2 by Moles et al. (1998), have a redshift $cz \sim 6020$ km s^{-1} (Moles et al. 1998), in good agreement with the motion of the H I gas in NW-LV. Redshifts reported by Plana et al. (1999) for their Hα sources 1–5 near the H I peak also have radial motions between 5950 and 6005 km s^{-1}. Most of the Hα sources with measured velocities have radial motions very similar to the H I gas in NW-LV, which has the smaller velocity dispersion (Table 4). The mean radial velocity of the ionized gas is consistent with the H I motions in both of the NW features (Figs. 9*b* and 8*b*) and suggests that the H I gas and the ionized gas are physically related and are part of the same large structure.

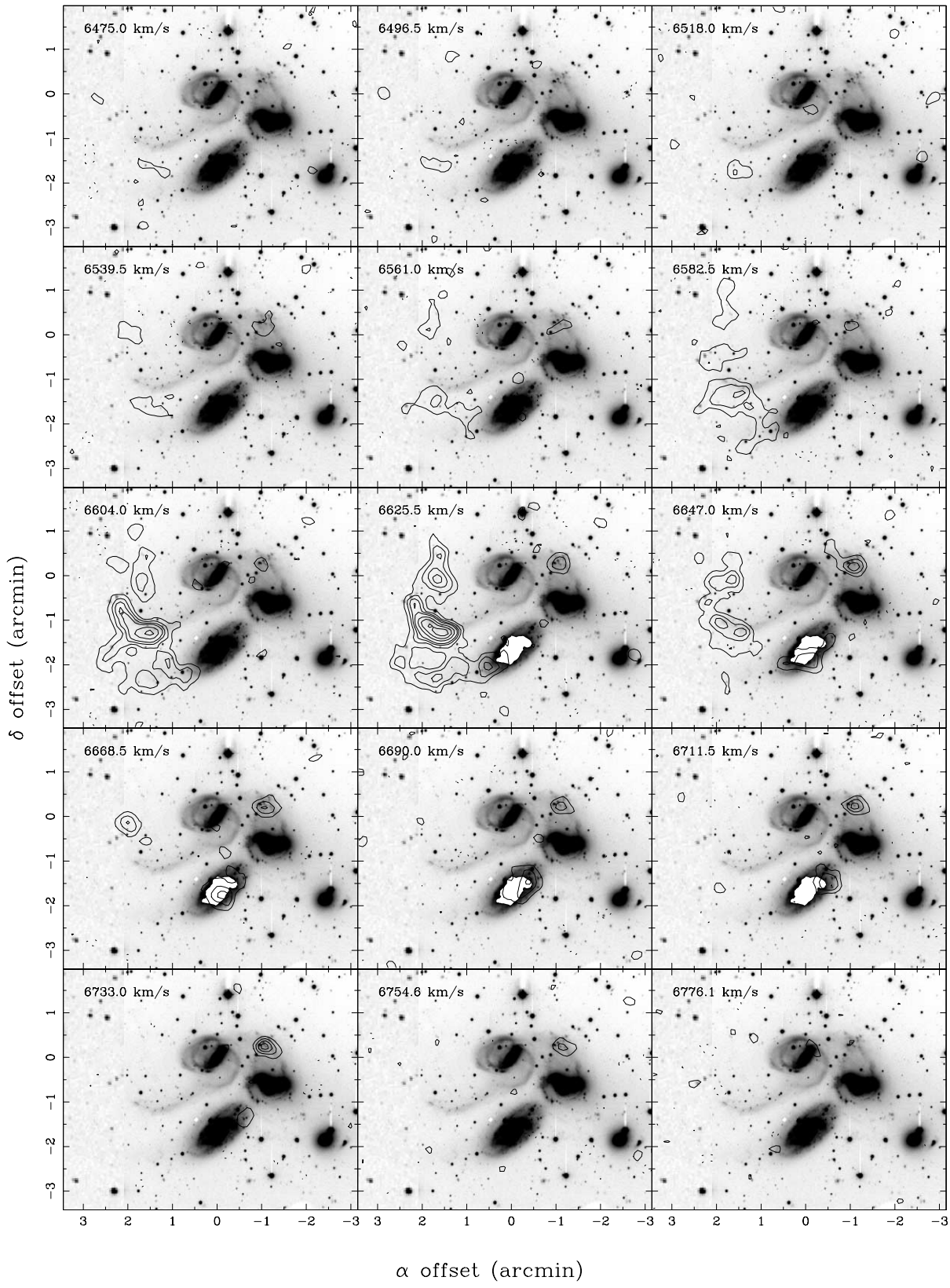

FIG. 7.—Channel maps of the 21 cm line radiation of HCG 92 corresponding to Fig. 8 superposed on the same *R* image as in Fig. 1. The POSS image has been used for the eastern part of the field. The contours are −3.4, 3.4, 6.9, 10, 14, 20, 27, and 34 × 10^{18} atoms cm^{-2}.

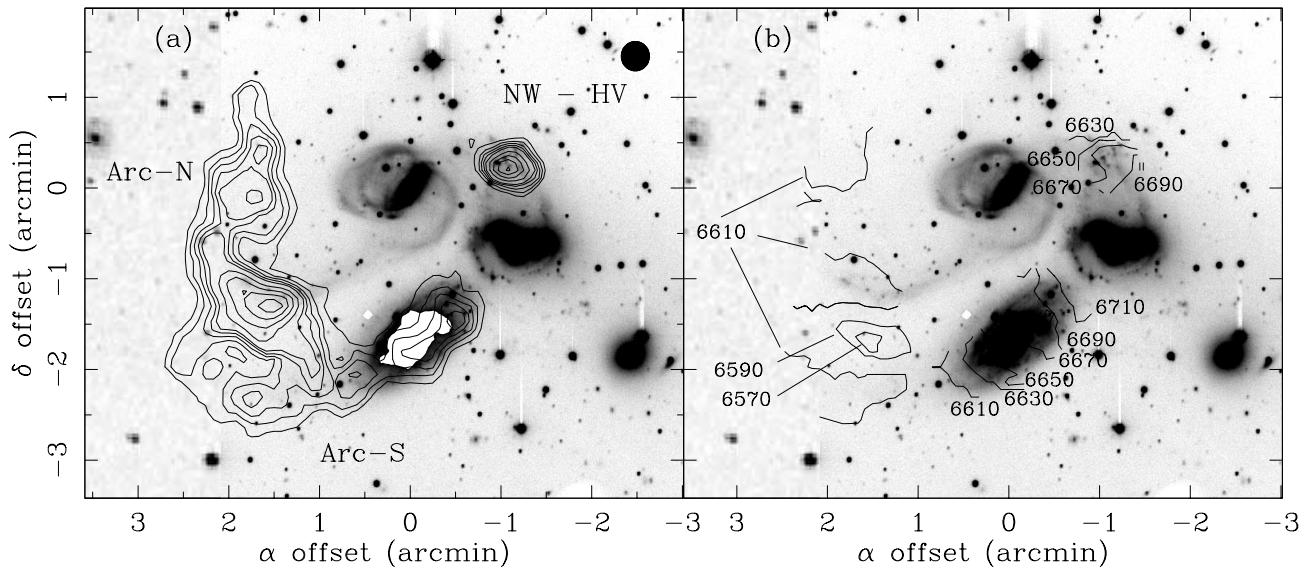

FIG. 8.—(*a*) Map of the H I column density distribution in HCG 92 in the velocity range 6475–6755 km s^{-1} superposed in the same *R* image shown in Fig. 1. The POSS image has been used for the eastern part of the field. The contours are 5.8, 12, 18, 23, 29, 44, 58, 73, and 87 × 10^{19} atoms cm^{-2} and the synthesized beam is 19″.4 × 18″.6. (*b*) Map of the first-order moment of the radial velocity field. The numbers indicate heliocentric velocities in kilometers per second.

5.1.3. *Southwest Feature*

The remaining H I detected toward the quintet resides in a diffuse cloud just south of NGC 7318A/B (Fig. 11). This feature was originally detected by Shostak et al. (1984), who named it "West B", and we identify it as the SW component in Table 4. With the IF band centered at 1394.3 MHz (5597 km s^{-1}), we successfully detected emission in 10 velocity channels (Fig. 12). The systemic velocity of the SW feature is at 5700 km s^{-1} (Table 4) and is consistent with the value obtained by Shostak et al. (1984). Both the velocity integrated H I image (Fig. 11) and the channel maps (Fig. 12) suggest that this feature consists of two large clumps. The northern clump spatially coincides with the tidal feature seen just south of NGC 7318A and a second stream of tidal features and Hα sources seen further south. The second clump is located about 1′ (25 kpc) south, and no stellar or Hα emission are associated with it.

The H I peaks of the SW feature have a much lower column density than the peaks associated with the other three

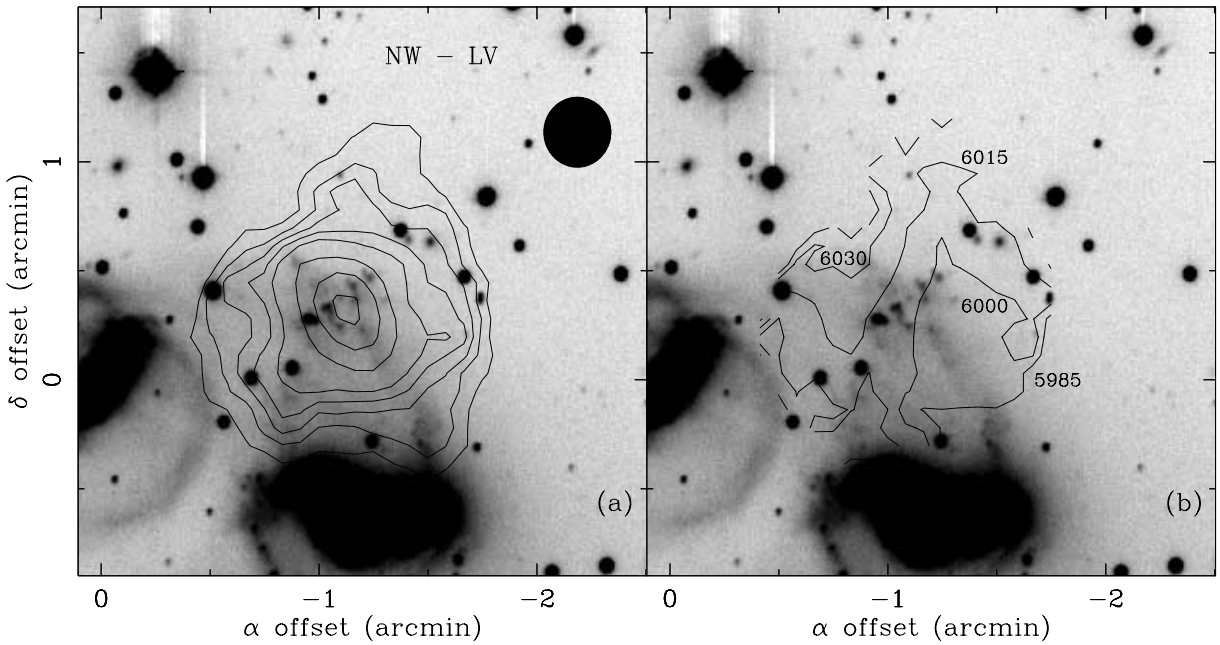

FIG. 9.—(*a*) Map of the H I column density distribution in HCG 92 in the velocity range 5959–6068 km s^{-1} superposed in the same *R* image shown in Fig. 1. The POSS image has been used for the eastern part of the field. The contours are 5.8, 12, 18, 23, 29, 44, 58, and 73 × 10^{19} atoms cm^{-2} and the synthesized beam is 19″.4 × 18″.6. (*b*) Map of the first-order moment of the radial velocity field in the same velocity range as in Fig. 9*a*. The numbers indicate heliocentric velocities in kilometers per second.

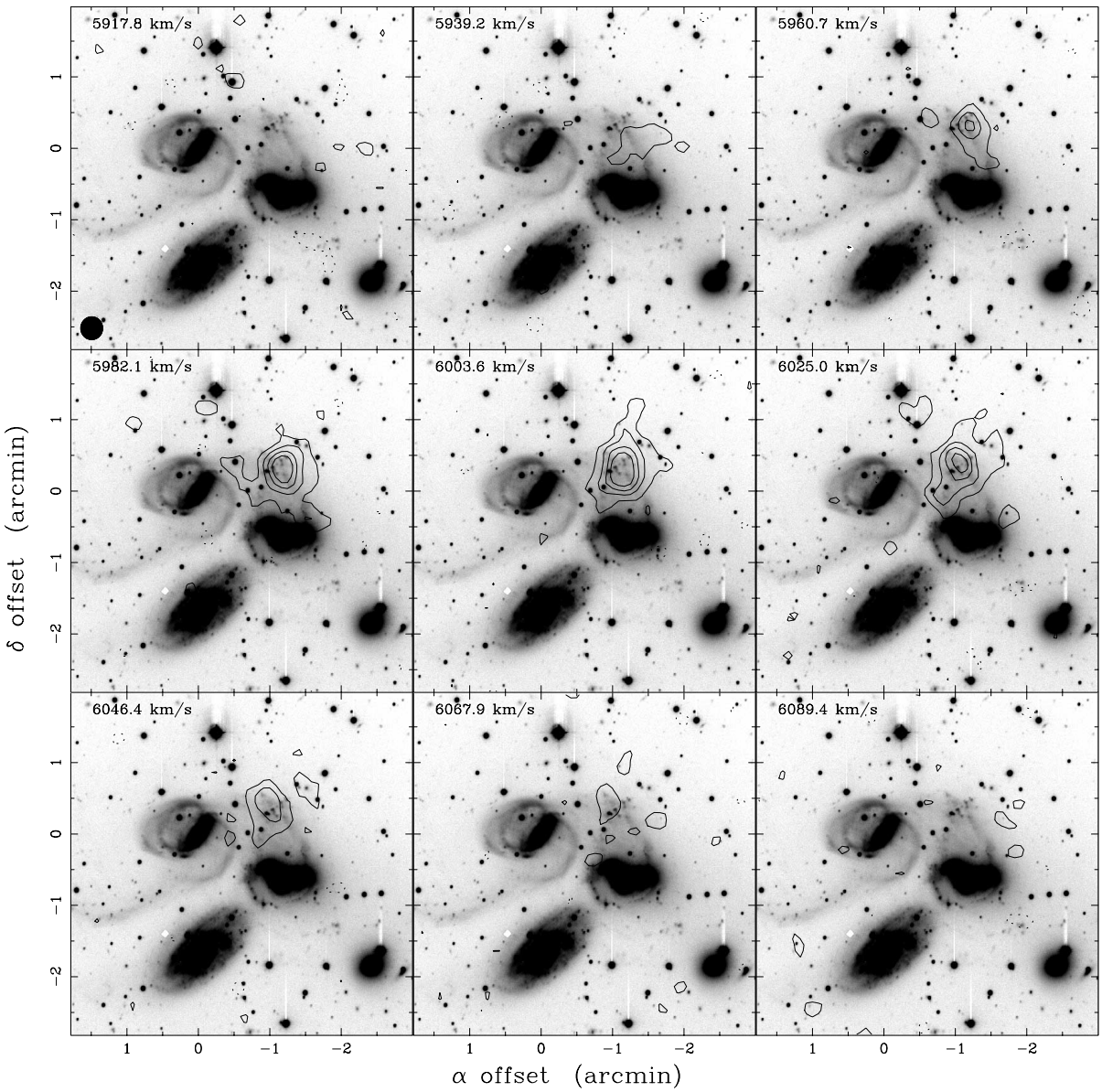

FIG. 10.—Channel maps of the 21 cm line radiation of HCG 92 corresponding to Figure 9 superposed on the same R image as in Figure 1. The POSS image has been used for the eastern part of the field. The contours are -3.4, 3.4, 6.9, 10 and 14×10^{18} atoms cm^{-2}.

TABLE 4

H I PARAMETERS[a] OF THE KINEMATICAL COMPONENTS

Parameter	SW	NW-LV	NW-HV	Arc-S	Arc-N
$\langle V_{\rm HI}\rangle$ (km s^{-1})	5699 ± 15	6012 ± 10	6647 ± 15	6641 ± 10	6604 ± 10
Velocity width (km s^{-1})	213 ± 5	160 ± 5	255 ± 5	153 ± 5	114 ± 5
Size (arcmin)	1.5×0.9	1.2×1.0	0.7×0.5	3.1×0.7	3.6×1.3
Size (kpc)	37×22	30×25	17×12	77×17	89×32
Peak flux (Jy km s^{-1})	0.14 ± 0.01	0.26 ± 0.01	0.31 ± 0.01	0.11 ± 0.01	0.33 ± 0.01
Peak $N_{\rm H\,I}$ (10^{21} cm^{-2})	0.41 ± 0.03	0.76 ± 0.03	0.90 ± 0.03	0.32 ± 0.03	0.96 ± 0.03
Peak A_V (mag)	0.20	0.36	0.46	0.46	0.25
Integrated flux (Jy km s^{-1}):					
Shostak et al. 1984	1.3 ± 0.3	1.7 ± 0.2	10.5 ± 1.0	...	...
New VLA	0.87 ± 0.13	1.30 ± 0.20	0.52 ± 0.08	1.48 ± 0.20	2.63 ± 0.40
$M_{\rm HI}$ ($10^9 M_\odot$)	1.5 ± 0.2	2.2 ± 0.3	0.9 ± 0.1	2.5 ± 0.4	4.0 ± 0.6

[a] Assuming distance of 85 Mpc for SQ.

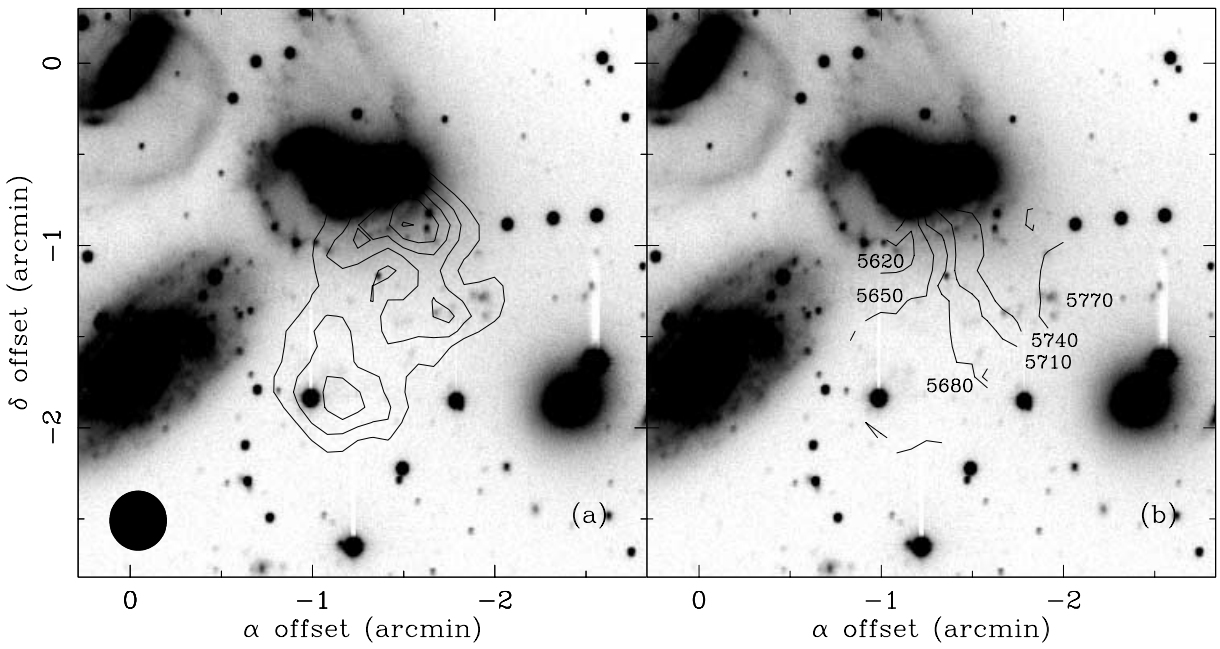

FIG. 11.—(*a*) Map of the H I column density distribution in HCG 92 in the velocity range 5597–5789 km s^{-1} superposed in the same *R* image shown in Fig. 1. The POSS image has been used for the eastern part of the field. The contours are 5.8, 15, 23, 32, and 41 × 10^{19} atoms cm^{-2} and the synthesized beam is 19″.4 × 18″.6. (*b*) Map of the first-order moment of the radial velocity field in the same velocity range as in Fig. 11*a*. The numbers indicate heliocentric velocities in kilometers per second.

major features (Table 4). As in the NW feature, the H I peaks in the SW feature also appear to coincide closely with the Hα objects B3 and B4 from Arp (1973) or 15 and 14 in Plana et al. (1999). Taken on its own, the velocity field seen in Figure 11*b* is similar to that of a distinct, rotating galactic disk. The motions of the gas are not compatible with those measured near the nucleus of NGC 7318A (Moles et al. 1998). Instead, the gas velocity field is closer to the radial motions in NGC 7318B.

The images shown in Figure 11 and 12 provide greater detail in the distribution and kinematics of the H I than is available in the corresponding Westerbork maps (Shostak et al. 1984) and reveal for the first time that the SW component is clearly distinct and separate from the other H I features. When taken together, the unrelated velocity gradients across the low-velocity features, i.e., NW-LV and SW components (Table 4), do not support the Moles et al. (1997) model of a single rotating disk of H I that is gravitationally bound to NGC 7318B. It is clear from the VLA H I data that the lower velocity gas emanates from two structures that are spatially and kinematically distinct.

5.1.4. *Summary of the* H I *Features*

The new VLA observations improve our understanding of the nature and extent of the atomic gas in SQ. The distribution of the H I gas detected with the VLA follows very closely the high surface brightness features present in the WSRT data. The large eastern cloud resolves into 2 kinematically distinct features that coincide with the optical tidal tails that extend eastward toward NGC 7320C. It is now clear that the two low-velocity clouds in the western part of SQ are physically and kinematically distinct from each other and the rest of the cloud features. The presence of ionized gas traced in Hα, coincident both in location and velocity, is ubiquitous for all H I features.

All but one bright structure present in the WSRT data are confirmed. The one exception, found just south of NGC 7819 in the WRST map, is puzzling. Given the VLA's flux density and surface brightness sensitivities, this source should have been confirmed at the ~20 σ level. The WSRT data by Shostak et al. (1984) was affected by radar interference, and this feature may be a resulting artifact (see below).

5.2. *Integrated Profiles of Distinct Regions in the Quartet*

In order to investigate the global properties of the components described above, we produced integrated line profiles of the H I emission within the four regions shown in Figure 5. The integrated profiles of NW-LV, NW-HV, SW, Arc-S, and Arc-N, shown in Figure 13, have been reconstructed point by point from the individual channel maps (Figs. 7, 10, and 12). Table 4 lists the relevant parameters of these line profiles along with the integrated fluxes determined directly from the H I spectra (Fig. 13), the total hydrogen masses for each feature, and the corresponding values from Table 2 of Shostak et al. (1984) for comparison.

The most peculiar H I profile shape obtained in the direction of Arc-S (see Fig. 13) is remarkably similar to the Arecibo H I profile measured by Peterson & Shostak (1980) in their direction "SSWW" just south of NGC 7318A/B and west of NGC 7320. This asymmetric profile shape is generated by the high-velocity gas in the faint tail behind NGC 7320, where the motions are observed to be very systematic (Fig. 6*b*). Since the line shape cannot be attributed to irregularities in the velocity field, this result suggests that there is more H I in the southeastern end of the tidal tail than toward the northwestern edge where the continuum ridge begins. In region Arc-N, the line profile (Fig. 13) has its smallest width and most symmetric shape illustrating how uniform the motions are over this extended region. These motions can be understood if we are observing a sheetlike

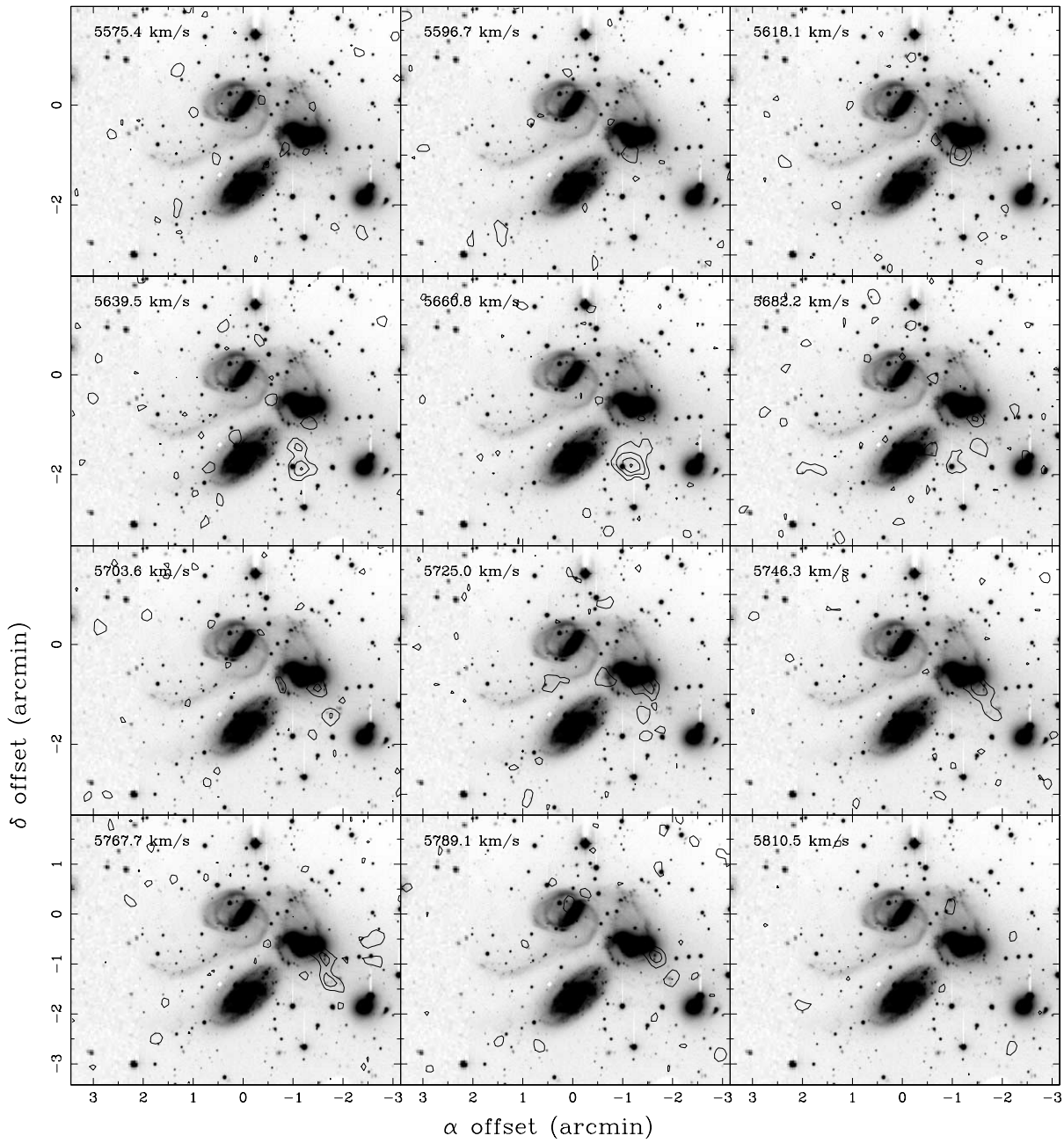

FIG. 12.—Channel maps of the 21 cm line radiation of HCG 92 corresponding to Fig. 11 superposed on the same *R* image as in Fig. 1. The POSS image has been used for the eastern part of the field. The contours are −3.4, 3.4, 6.9, 10, and 14 × 10^{18} atoms cm^{-2}.

distribution with its thin axis oriented mostly along the line of sight. Any large-scale motions, if present in this feature, would occur mostly in the plane of the sky and not along the line of sight, where random motions are expected to be small given the three-dimensional distribution of tidal features.

The broadest profile is measured in the direction of NW-HV, where strong Hα and mid-IR sources (Xu et al. 1999) are also present near the end of a tidal feature that may belong to NGC 7318A (Plana et al. 1999). There are fewer Hα emission sources at the radial velocity of NW-HV than at the lower velocity of the NW-LV component. This combination of high column density and large velocity width measured for NW-HV (Table 4) could be produced by a projected structure with significant bulk motion along the line of sight. Alternatively, NW-HV could be a self-gravitating complex star-forming region on its way to becoming a dwarf galaxy and the large-scale motions may be an indication of its rotation. Zwicky (1956) was the first to introduce the idea that self-gravitating objects in tidal tails could evolve into dwarf galaxies. If NW-HV is a self-gravitating body, its dynamical mass is least 3.2 × 10^{10} $M_{\odot}$, given its unknown inclination. The neutral hydrogen measured in the direction of NW-HV would then account for no more than 3% of its total mass.

To facilitate comparisons with published spectra obtained with single-dish and other aperture-synthesis observations, we generated a composite spectrum (Fig. 13) of all the flux detected in the quintet (Fig 5). This spectrum

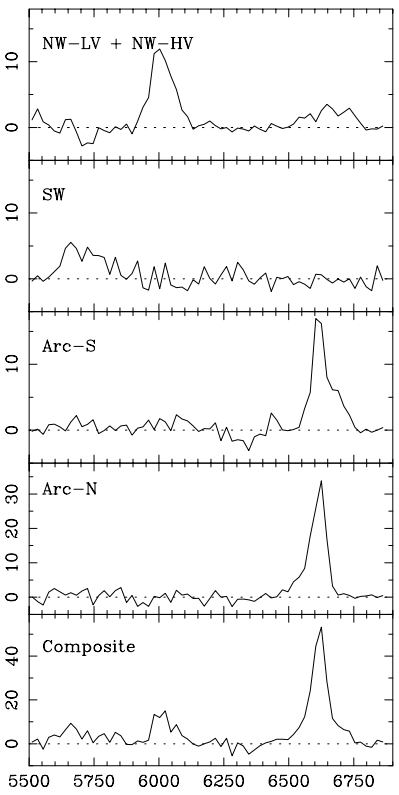

FIG. 13.—H I flux density in units of millijanskys as a function of heliocentric velocity in units of kilometers per second for the features indicated in each plot.

clearly shows, as expected, the three velocity components at 6600, 6000, and 5700 km s^{-1} with three emission peaks at ~55, ~15, and ~10 mJy, respectively. The distribution of the relative flux in Fig. 13 is nearly identical with those of spectra obtained with WSRT (Shostak et al. 1984), Arecibo (Gordon & Gordon 1979; Shostak 1974; Williams & Rood 1987), Nancay (Balkowski et al. 1973), and the NRAO 91 m (Williams & Rood 1987) telescopes, except that detection of the 5700 km s^{-1} component is at best marginal in most of the published profiles. Only the composite spectra of Shostak et al. (1984) and Peterson & Shostak (1980) show all three velocity components. The integrated flux reported by Peterson & Shostak (1980) and Shostak et al. (1984) for the 6600 km s^{-1} velocity component is at least a factor of 2 higher than the VLA measurement (Table 4). The 6000 and 5800 km s^{-1} velocity components have integrated fluxes that are also lower than their corresponding WSRT or Arecibo values, but the difference is much less than that measured for the high-velocity gas. If we are to believe their results, then between 50% and 60% of the flux is missing from the VLA observations, most of which can be attributed to the high-velocity gas.

This large discrepancy cannot be accounted for by differences in the sensitivity or in the minimum spatial frequencies sampled by the two configurations. The WSRT high-resolution map has a synthesized beam (FWHP) of $24'' \times 47''$ and the brightness sensitivity in the final channel maps is 6.8×10^{-4} mJy $arcsec^{-2}$. The corresponding brightness sensitivity in the final maps of the VLA is 7.9×10^{-4} mJy $arcsec^{-2}$. The shortest baselines included in the VLA and WSRT observations are both ~30 m; therefore, smoothly distributed emission features with a size about 10′ and larger are missed by both instruments and do not contribute to the flux. Close inspection of the WSRT composite spectrum (Fig. 7*a*; Shostak et al. 1984) reveals a narrow high-velocity profile on top a strongly curved baseline from 5300 to 7500 km s^{-1}, in contrast to the very flat baselines present in the VLA spectra (Fig. 13). Baseline problems seen in an interferometric spectrum usually indicate a calibration or imaging problem with the data. Shostak et al. (1984) reported that 15 out of 63 total channels in their data were corrupted by radar interference. Although they claimed to have removed affected data, even low-level residual interference signal would affect the resulting images, particularly at the largest spatial scales, resulting in extended negative sources or displacement of emission peaks (e.g., see § 5.1.1). This might be enough to explain all observed discrepancies.

Over the last 30 years SQ has been observed with at least five different radio telescopes, three of which are single-dish antennas. Comparisons of the integrated flux measured with smaller single-dish antennas could give some indication of how much flux, if any, was missed with the synthesis array. Figure 14 shows a plot of the integrated flux measurements of the high-velocity gas as a function of telescope beam. We have chosen to compare the high-velocity gas because it was detected in all the published H I observations and, given its extended distribution, would more likely be affected by the sensitivity limitations and beam attenuation.

The beam areas plotted in Figure 14 span roughly 2 orders of magnitude, and most of the integrated flux values lie between 3.2 and 6.5 Jy km s^{-1}, consistent with the VLA measurement given uncertainties in receiver noise, baseline fits to the underlying continuum emission, and flux-scale calibrations. The only measurement in Figure 14 commensurate with the higher WSRT value is the one derived from an Arecibo composite spectrum (Peterson & Shostak 1980) generated from individual observations made over a grid centered on the group. Their low-resolution contour map (Plate L1; Peterson & Shostak 1980) shows H I emission that extends over ~8′ at an integrated brightness of 8 K km s^{-1} $beam^{-1}$ or 0.94 Jy km s^{-1} $beam^{-1}$ and fills a region as large

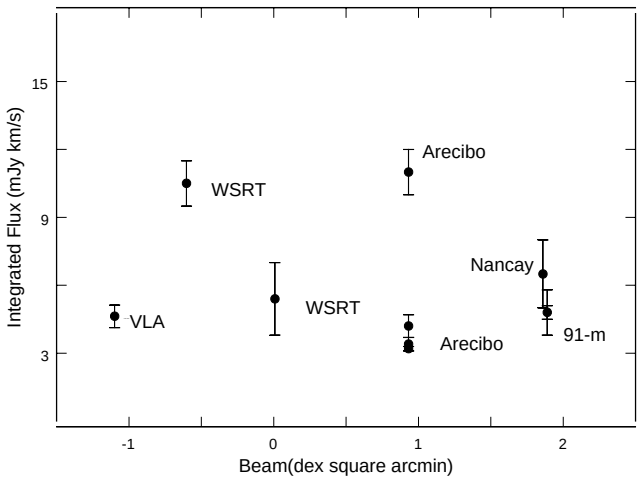

FIG. 14.—VLA and published H I integrated fluxes of the high-velocity gas between 6475–6755 km s^{-1} as a function of telescope beam area in units of square arcminutes on a logarithmic scale. Values measured with Arecibo, NRAO 91 m, Nancay, WSRT, and the VLA radio telescopes are labeled for comparison.

as 6.5 Arecibo beams. None of the emission detected with the VLA or with WSRT is observed to be this extended; however, the Arecibo observations are more sensitive, i.e., $\sim 10^{-5}$ mJy arcsec^{-2}. If we assume that the Arecibo map is representative of the true source brightness, then a velocity width of 280 km s^{-1} (Peterson & Shostak 1980) would give an average brightness of 10^{-4} mJy arcsec^{-2} for the most extended emission. This is well below the brightness sensitivity of both WSRT and the VLA. Given similar reported values of the integrated flux, it is difficult to understand how WSRT could have detected the same faint emission present in the Arecibo map.

The most sensitive observations with the NRAO 91 m telescope (Fig. 14) were made by Williams & Rood (1987); their H I spectrum has an rms noise per channel of 2.9 mJy, which is roughly a factor of 10 higher than the noise in the Arecibo spectrum. But the NRAO 91 m beam is a factor of 10 larger, resulting in a sensitivity $\sim 10^{-5}$ arcsec^{-2}. Because the NRAO 91 m and the Arecibo telescopes have similar sensitivities, the NRAO 91 m observations can provide an independent check of the larger Arecibo measurement of the integrated flux and a confirmation of the extended emission. The faint emission present in the Arecibo map fills a region that is $\sim$70% of the NRAO 91 m half-power beam. Williams & Rood (1987) report an integrated flux of 4.8 ± 0.3 Jy km s^{-1} which is consistent with the value measured by Shostak (1974) but less than half of the highest reported Arecibo measurement.

The faint emission in the Arecibo map accounts for 56% of the total integrated flux measured by Peterson & Shostak (1980). In order to avoid detection with the NRAO 91 m telescope, the faint emission would have to be distributed well outside of the HPBW, which is inconsistent with the angular distribution of the high-velocity gas in both the WSRT and Arecibo maps. Although sensitive to the faint emission in the Arecibo map, the NRAO 91 m telescope is unable to confirm this detection and raises doubts about whether the 8 K km s^{-1} emission present in the Arecibo is real or an artifact of beam smearing. It is worth noting that emission as bright as 16 K km s^{-1} in the Arecibo map matches in angular extent the H I detected with both the VLA and WSRT and has an integrated flux of 4.8 Jy km s^{-1}, consistent with the measurements made with both the VLA and the NRAO 91 m telescope.

In summary, the observed line widths of the components detected in the direction of the quintet are all very small, less than 270 km s^{-1}. Their angular extent tends to correlate inversely with line width; i.e., the most compact component, NW-HV, has the largest line width, while the most extended feature, Arc-N, has the smallest (Table 4). This correlation may be related to how dynamically evolved each feature is. NW-HV is coincident with that of known Hα emission regions or dwarf galaxy candidates (Hunsberger et al. 1996) and its larger line width may be an indication of a local density enhancement and a deeper gravitational potential. The integrated fluxes measured with the VLA are all lower than their corresponding WSRT values. There is more than a factor of 2 difference between the two measurements of the high-velocity gas near 6600 km s^{-1}. This discrepancy cannot be explained by differences in sensitivity or in the limitations on the minimum spatial frequencies that can be mapped by each instrument. In contrast, the VLA measurement of the total integrated flux is in good agreement with single-dish measurements made with Arecibo, Nancay, and the NRAO 91 m telescopes.

6. NEIGHBORING GALAXIES

It is not surprising that we detected three other galaxies within the primary beam, since SQ is not isolated, with NGC 7320C, its closest bright neighbor, less than 5′ from the quartet's center. Tammann (1970) was one of the first to point out that SQ is probably part of the Zwicky Cluster $22^{\rm h}31\overset{\rm m}{.}2+37^\circ 32'$ (Zwicky & Kowal 1968). The five anonymous galaxies detected by Shostak et al. (1984) in the surrounding field support the idea that SQ is embedded in a much larger aggregate of galaxies. An integrated map of the H I between 5900 and 6750 km s^{-1} in the surrounding region (Fig. 15) shows the position of the three faint neighbors we detected. Two of the galaxies at $\alpha_{1950.0} = 22^{\rm h}33^{\rm m}34^{\rm s}$, $\delta_{1950.0} = 33^\circ 53' 53''$ and at $\alpha_{1950.0} = 22^{\rm h}34^{\rm m}23^{\rm s}$, $\delta_{1950.0} = 33^\circ 41' 17''$ had already been detected by Shostak et al. (1984) and named "Anon. No. 2," and "No. 4," respectively, in their list of five. This earlier detection of H I in Anon. No. 2 was quite marginal, but we are able to confirm H I emission in both these galaxies and add a newly detected neighbor, Anon. No. 6, at $\alpha_{1950.0} = 22^{\rm h}34^{\rm m}56^{\rm s}$, $\delta_{1950.0} = 33^\circ 49' 25''$.

The H I emission associated with Anon. No. 2 is seen in just three channels. The emission peak coincides with the optical galaxy, as shown in the left part of Figure 16*a*. H I emission in Anon. No. 2 is centered near 6380 km s^{-1} and has a peak H I column density of 6.3×10^{20} atoms cm^{-2}. The observed velocity gradient across this galaxy is rather shallow (Fig. 16*a*, *right*) but consistent with a rotating disk viewed nearly face-on. Anon. No. 4 has H I emission that is quite symmetrical (Fig. 16*b*, *left*) and rotation is evident in the channel maps that clearly show the position of the H I centroid displaced along the same position angle as that of the galaxy's principal axis (Fig. 16*b*, *right*). This is consistent with motions generated by an inclined rotating disk of gas. As in Anon. No. 2, the distribution of the H I in Anon. No. 6 is asymmetric with respect to the center of the galaxy (Fig. 16*c*, *left*); however, the major axis of the H I emission follows, rather constantly, the position angle of the optical disk (Fig. 16*c*, *right*). The optical and H I properties of the faint galaxies detected in the field surrounding SQ are summarized in Table 5.

7. DISCUSSION

New synthesis observations have motivated us to reassess previously published results and revise dated images that have characterized the H I morphology of SQ for nearly 20 years. The new observations at higher angular and velocity resolutions than any published results to date provide far more details about the internal motions of the H I gas in SQ and allow direct comparisons between H I emission and other discrete and extended sources within the group over a range of wavelengths, i.e., X-ray, optical, Hα, continuum, and infrared.

The higher resolution of the VLA has provided us with additional clues about the short-term consequences of collisions and interactions, as well as the dynamical history of the high-redshift members in the quintet. New details on substructures within all H I features detected, including the foreground galaxy NGC 7320 and the H I cloud at 6600 km

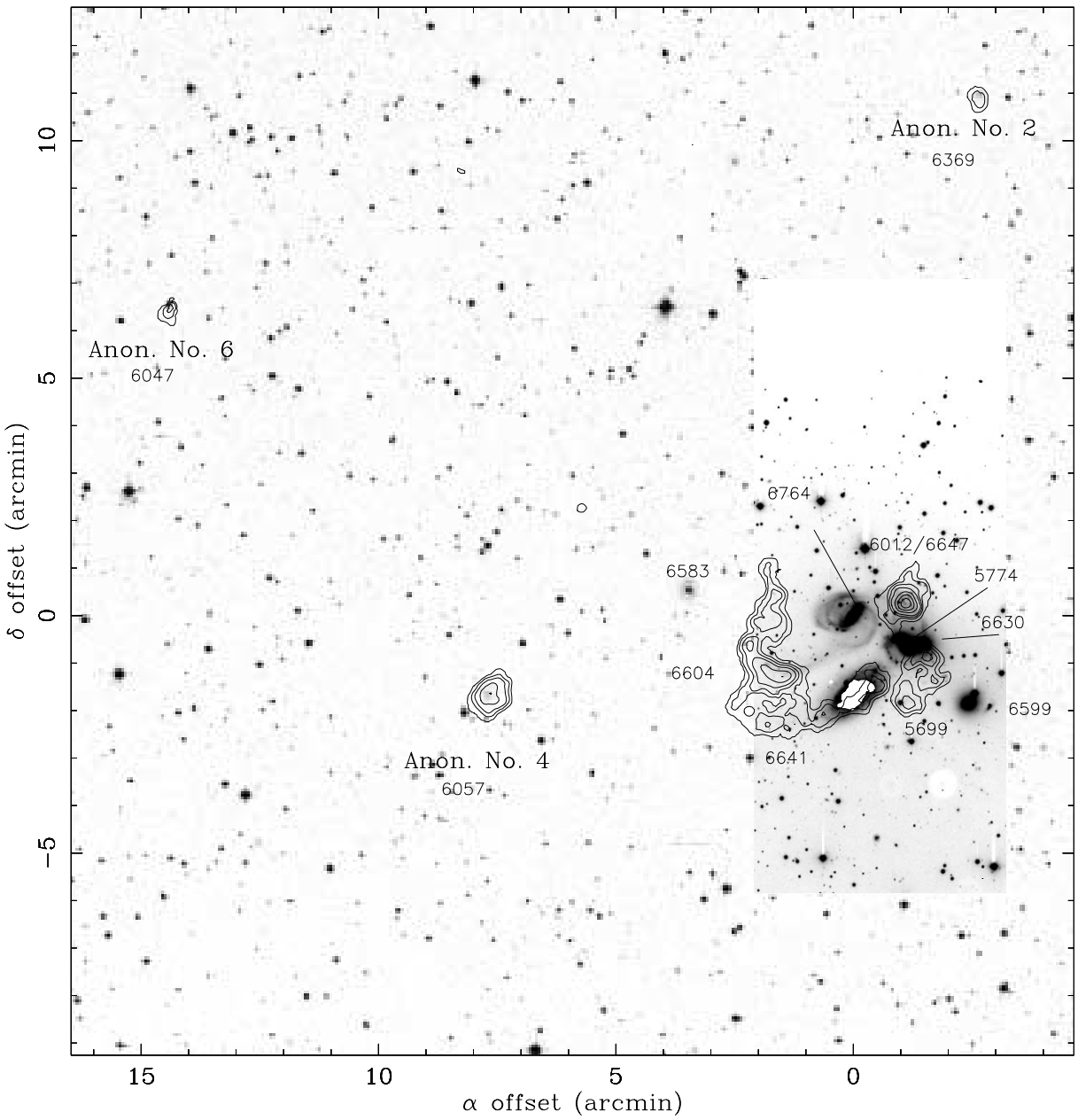

FIG. 15.—Map of the H I column density distribution in HCG 92 superposed on the same *R* image shown in Fig. 1 for the central part and the POSS image for the rest of the field. The contours are 5.8, 13, 22, 35, 61, 87, 117, and 150 × 10^{19} atoms cm^{-2}. The systemic velocities of the H I features (Table 4), the satellite galaxies (Table 5), and the bright galaxies (Hickson 1992; Sulentic et al. 2001) are labeled.

s^{-1}, hold the valuable clues about the dynamical history of the group.

7.1. *Gaseous Collisions in the Group*

The large velocity difference of NGC 7318B with respect to the rest of the group ($\Delta V \sim 700$ km s^{-1}) has been taken as key evidence for its being an intruder passing through the group. A collision at such a high velocity would result in widespread shocked and ionized regions, followed by rapid cooling due to the emission of radiation at UV and X-ray wavelengths (e.g., Harwit et al. 1987). The radio continuum ridge found east of NGC 7318B has been suggested to be the interface between the interloper and the group, because the shocked, ionized gas is predicted to produce significant amounts of synchrotron emission (van der Hulst & Rots 1981; Allen & Hartsuiker 1972). The synchrotron life time for the radiating electrons is estimated to be rather short, a few times 10^7 yr, which is comparable to the crossing time for such a collision.[3] The presence of extended, diffuse X-ray emission associated with the group (Sulentic et al. 1995; Pietsch et al. 1997) also raises the possibility that what is seen in SQ is the result of a collision between a galaxy and a

[3] A classic example of enhanced radio synchrotron emission arising from a collision involving two galaxies is the "Taffy" pair (UGC 12914/5; Condon et al. 1993). The H I observations of this colliding system should also help in understanding the response of cold gas within the progenitor's disks (see below).

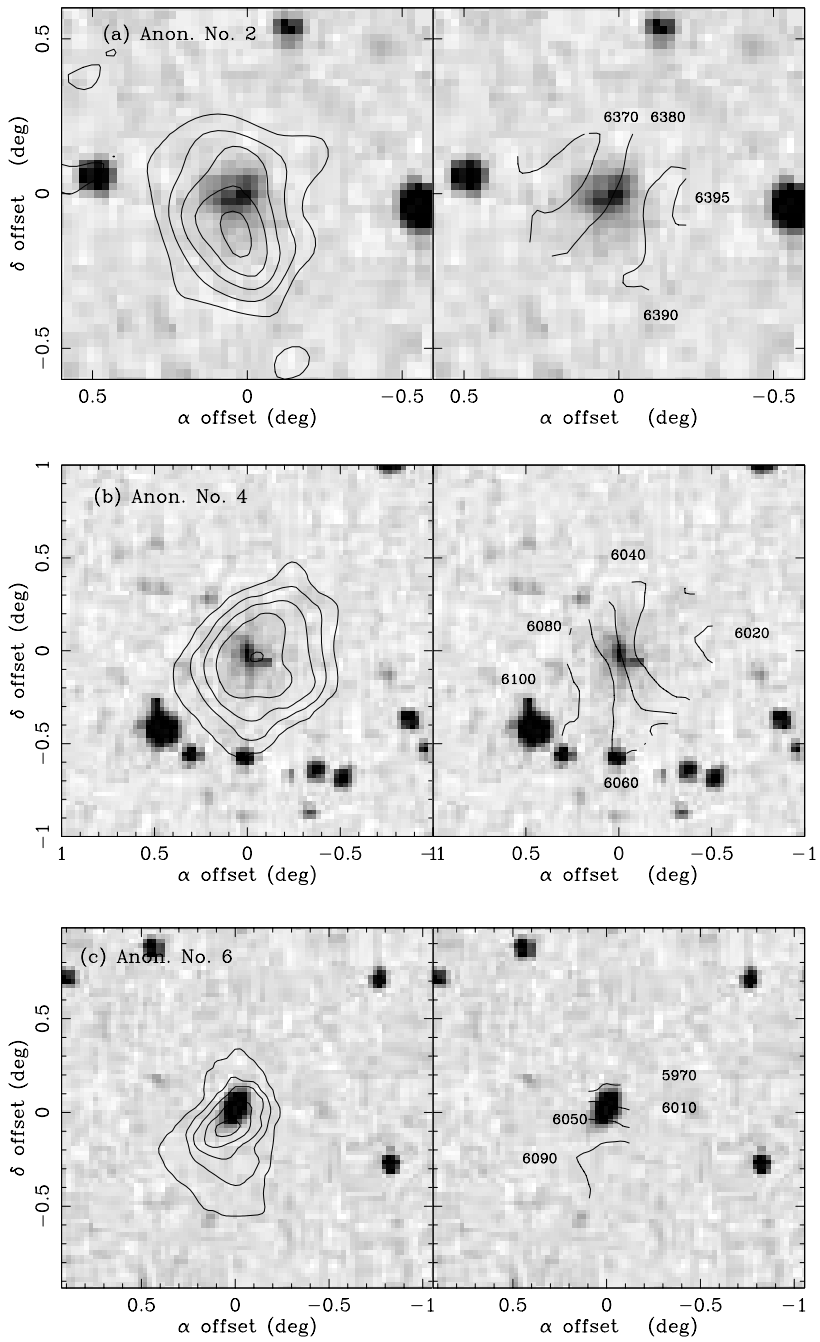

FIG. 16.—Map of the H I column density distribution (*left*) and first-order moment of the radial velocity field (*right*) of satellite galaxies (*a*) Anon. 2 (*b*) Anon. 4, and (*c*) Anon. 6 superposed on the POSS image. The column density contours are (*a*) 15, 26, 37, 48, and 59 × 10^{19} atoms cm^{-2}; (*b*) 7, 13, 20, 26, and 33 × 10^{19} atoms cm^{-2}; and (*c*) 4, 13, 22, 31, and 40 × 10^{19} atoms cm^{-2}. The synthesized beam is 17″.5 × 16″.8. The numbers in the radial velocity field indicate heliocentric velocities in kilometers per second and the velocity contours are in units of 10 km s^{-1}.

TABLE 5

SATELLITE GALAXIES

Anon. No.	Size[a] (arcmin)	Type	$V_\odot$ (km s^{-1})	$\int S_v dv$ (Jy km s^{-1})	ΔV_{20} (km s^{-1})	$M_{\rm H\,I}$ ($10^9\ M_\odot$)
2.....	0.45 × 0.20	Sc	6369 ± 10	0.32 ± 0.05	86 ± 10	0.54 ± 0.08
4.....	0.35 × 0.10	SB	6057 ± 10	0.70 ± 0.10	129 ± 10	1.08 ± 0.20
6.....	0.20 × 0.10	S	6047 ± 10	0.22 ± 0.03	65 ± 10	0.34 ± 0.05

[a] Sizes were measured on the blue POSS print.

hot group medium. Given the n_e^2 dependence on emissivity, such a collision should be much less effective in producing radio continuum emission than would be a collision involving two galaxy disks. A logical place to look for such an example is the centers of nearby clusters, such as Virgo and the Coma Clusters, and NGC 4522 may be an example of such a collision between diffuse cluster/group medium and a galactic disk (Kenney & Koopmann 1999; Kenney et al. 2000). Though plausible, such objects are rare in clusters, and the tenuous intragroup medium in SQ would weaken the case considerably.

The excellent surface brightness sensitivity achieved by our new observations reveals several new details for the first time, including the faint structure in the extended radio ridge between NGC 7318B and NGC 7319. As seen in Figure 1, the continuum ridge approximately follows the optical tails. The new continuum image also raises minor issues for the hypothesis that the extended radio continuum ridge, also visible in X-ray and Hα, is the product of a collision involving NGC 7318B. Because NGC 7318B sits in the middle of the ridge its trajectory has to be mainly in the direction perpendicular to the extent of the ridge; however, the shape of the radio ridge is S shaped and not the expected symmetric C shape of a bow shock.

A careful comparison of radio continuum and Hα images by Ohyama et al. (1998) shown in Figure 17 reveals some important differences. The morphology of the Hα emission is indeed C shaped, more in line with the shock hypothesis. This apparent discrepancy may be resolved at least in part by the difference in the radiation timescales. The cooling time for the Hα emitting gas is much shorter than the synchotron lifetime for the radio-emitting electrons, and Hα is tracing only the most active, ongoing shocked regions. There is also some evidence that more than one source of Hα emission may be present. The continuum subtracted line image centered at 6738 Å (including both Hα and [N II] emission) by Sulentic et al. (2001) resembles our radio continuum image more closely, and the radio continuum may be tracing mainly the ionized gas at a the higher velocity (i.e., 6600 km s^{-1}) as shown in Figure 2 of Xu et al. (1999).

The striking morphological alignment between Hα and the H I features near 6600 km s^{-1}, shown in the right panel in Figure 17, raises an intriguing possibility that NGC 7318B may be colliding with part of the H I tidal tail of Arc-S that runs behind NGC 7320. Implicit in this hypothesis is that this H I tail may be linked with the NW-HV feature, and the missing segment in H I may be fully ionized and visible only in Hα and in radio continuum. The recession velocity of the ionized gas in the southern parts of the Hα filament measured by Ohyama et al. (1998) is around 6600 km s^{-1}, consistent with this scenario. Further, the broad line width ($\Delta v \sim 900$ km s^{-1}) measured by Ohyama et al. (1998) is also consistent with such a collision scenario.

7.2. *Star Formation Activities in SQ*

Examples of close correspondence between Hα emission and H I are found throughout SQ (see § 5.1). The two prominent star-forming complexes identified in mid-IR by Xu et al. (1999) are associated with two bright Hα complexes, and they both coincide with the two highest H I column density peaks (Arc-N and NW-HV). The H I peaks in the NW-HV, NW-LV, and the SW features all have associated Hα features, and the molecular gas complexes traced in CO by Yun et al. (1997) and by Gao & Xu (2000) are also associated with Hα features detected by Plana et al. (1999), Moles et al. (1998), Ohyama et al. (1998), Sulentic et al. (2001), and others.

Frequent tidal encounters in high-density regions are thought to be conducive to star formation activity, and indeed evidence for induced star formation activity is ubiquitous everywhere in SQ where cold gas is found. The star formation activity, however, is not as spectacular as one might expect in isolated environments such as in interacting

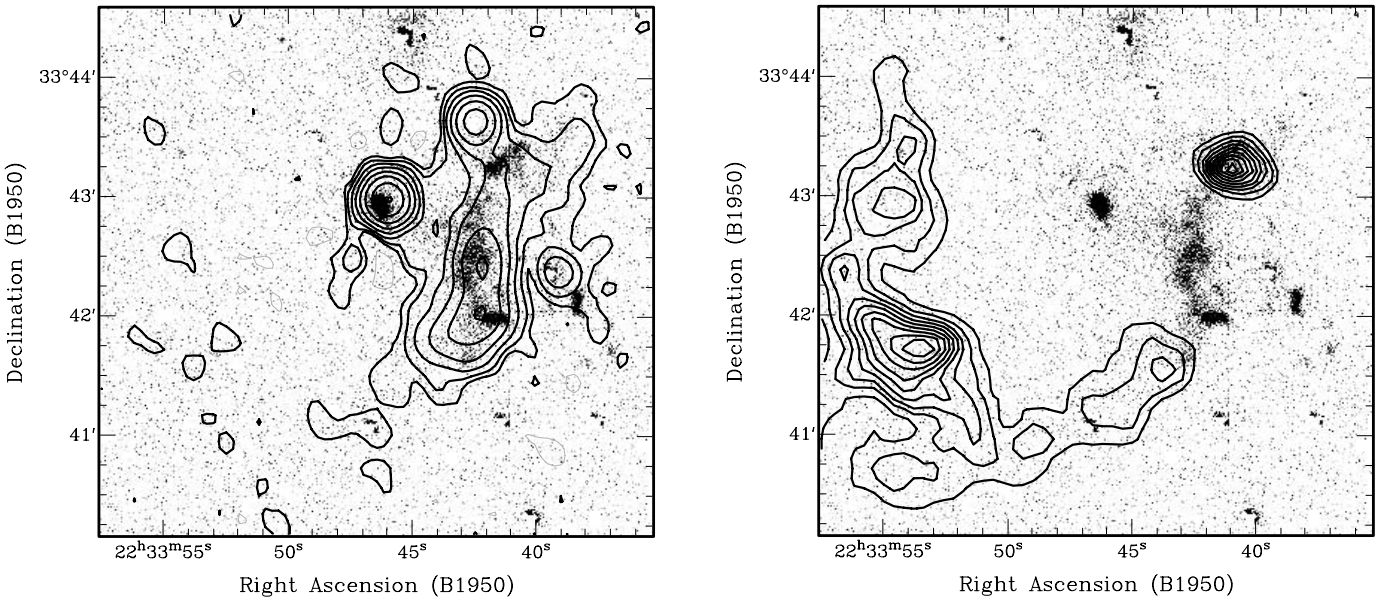

FIG. 17.—*Left*: Comparison of the radio continuum (in contours) with the Hα image by Ohyama et al. (1998). The contour levels are identical to those in Fig. 1. *Right*: Comparison of the H I column density distribution in HCG 92 in the velocity range 6475–6755 km s^{-1} (*in contours*) with the same Hα image. The contour levels are 10% of the peak.

pairs. Star formation is known to have a nonlinear dependence on gas density (e.g., Kennicutt 1998), and few high-density regions are currently present in SQ and little cold gas is remaining in the individual galaxies. These trends of low gas content and ubiquitous but suppressed star formation activity are commonly found in our examination of a large sample of Hickson compact groups (Verdes-Montenegro et al. 2001).

7.3. *Tidal Features and Interaction Scenarios*

The improved sensitivity and resolution of the new VLA data have significantly improved our understanding of the nature and distribution of the H I tidal features in SQ (see § 5.1). The massive L-shaped H I arc located about 3′ (75 kpc) east of SQ is shown to be possibly consisting of two separate tidal features (Arc-N and Arc-S in Fig. 6), in accordance with the two optical tails seen. Most of the gas in Arc-N is located near the end of the long sinuous tail emanating from NGC 7319. While Arc-N appears to originate from NGC 7319, the origin of the southern tail is uncertain. Both of the NW clouds are located near the tips of two crossing optical features north of NGC 7318A/B. The two NW features are quite distinct in velocity, but they appear spatially coincident exactly within our resolution. Therefore the two may be physically related. The SW feature at 5700 km s^{-1} is shown to be a distinct feature consisting of two to three clumps. If only its velocity field is considered, it might be an independent dynamical entity, such as a dwarf galaxy (see § 5.1.3).

One of the clear conclusions that can be drawn from the new data is that the 5700 km s^{-1} feature and 6000 km s^{-1} feature are clearly not the tidally disrupted disk of NGC 7318B, as proposed by Moles et al. (1998). In fact, none of the H I features are clearly associated with any of the individual galaxies. It is conceivable that in the past the two features could have been part of a single structure, possibly related to NGC 7318B, and separated into two distinct features forming the components we see today. Such a separation cannot be a direct outcome of a tidal disruption because *everything* within the tidal radius, including gas and stars, should have responded identically to the tidal shear. To the contrary, the core of the optical galaxy appears intact. The suggestion that NGC 7318B may be passing through the group for the first time (Moles et al. 1998; Sulentic et al. 2001) is certainly unlikely, especially if the observed X-ray, Hα, and radio continuum ridge is the evidence for the ongoing collision, because tidal damages due to such a collision, particularly the removal of outer gas and stellar disk and the development of the characteristic tidal tails, should form only after the closest encounter. Physical separation by a direct collision, though naively attractive, is not a likely explanation, because one cannot simply slice a gas cloud into two pieces. The face-on collision involving two disk galaxies in the "Taffy" pair resulted in only a slight rearrangement and displacement of the H I in both disks (Condon et al. 1993), without producing any dramatic consequences of the type speculated here.

The general proximity and relative orientation of NGC 7320C with respect to the optical and H I tails have been invoked as evidence for its recent passage through SQ and possibly as an explanation for the northern optical tail that appears to originate from NGC 7319 (e.g., Moles et al. 1998; Sulentic et al. 2001). Sulentic et al. (2001) even speculated that the two tidal tails might be the products of two consecutive passages by NGC 7320C. As clearly seen in various numerical studies of galaxy interactions (e.g., Barnes & Hernquist 1996), each passage by a companion generally erases all preexisting features, such as spiral arms and tidal tails, and such an explanation for the pair of tidal tails is probably not physical. Another common tendency seen in numerical simulations is that tidal tails generally point back to the responsible culprit, because the tidal debris and the passing companion have exchanged momentum, putting them in similar trajectories about the primary. This means the northern H I tail, at least the bulk of the segment pointing due north, *cannot be primarily driven by NGC 7320C*. The origin for the older (more diffuse and thicker) southern tail is also quite uncertain.

The number of faint neighbors with similar radial velocities as the galaxies in SQ is evidence that the quartet is not well isolated from the larger field of galaxies (see § 6). Therefore, interlopers may pass through and disturb the group with some frequency, including its H I companions such as Anon. 4. The resulting dynamical heating may be sustaining the group from collapsing (Governato et al. 1996), contrary to the prediction by Barnes (1996). One of the consequences of such a scenario is that interpreting the observed tidal features is no longer straightforward, as in interacting galaxy pairs. The high galaxy density in core of the group also means that any galaxy passing through the group is subject to multiple scatterings, rather than following a simple trajectory, and extrapolating the intuitions derived from the numerical studies of interacting pairs should be exercised with great caution.

An entirely different scenario one might consider, for at least parts of the observed H I features, such as the large arc feature, is that these are remnants of the primordial gas clouds where the group has formed out of or tidal debris formed during the initial formation of the group, similar to the Leo ring found around the M96 group (Schneider 1985; Rood & Williams 1985; Schneider et al. 1989). The Leo ring is a nearly complete ring of H I, with a diameter of about 200 kpc, thought to be orbiting the galaxies M105 (E0) and NGC 3384 (SB0) with a period of 4×10^9 yr. When examined at the same H I column density level of 9×10^{19} cm^{-2} shown in Figure 5, both the Leo ring and the H I arc feature are partial rings of H I of $\sim$100 kpc in size with linear velocity gradient perpendicular to their lengths. They both surround a group of galaxies interior to the ring and their systemic velocities match the galaxy group velocity. One significant difference is that at least parts of the H I arc in SQ have stellar counterparts, which rejects the primordial origin. The possibility that these rings of H I are remnants of group formation process, older than the group crossing time still seems plausible.

8. SUMMARY

Using C, CS, and D configurations of the VLA, we imaged five kinematically distinct H I clouds, a diffuse extended continuum ridge, and the disks of NGC 7320, and three faint dwarf galaxies in the direction of SQ. The most massive of the four clouds previously detected and confirmed by us is resolved into two separate systems, which accounts for the five clouds we report here. The two largest H I features east of the continuum ridge are coincident with and concentrated along the two large tidal tails that extend

toward the direction of the NGC 7320C. The two compact H I sources, west of the continuum ridge, have H I emission that peaks along the same line of sight and includes luminous infrared and bright Hα sources probably indicative of star formation activity in the densest regions of the gas. The fifth cloud, south of NGC 7318A/B, consists of two major clumps; one coincides with the tidal features south of NGC 7318a, and the other is devoid of any detectable stellar or Hα sources. As in previous H I studies, no emission was detected at the positions of any high-redshift galaxies including NGC 7320c; any H I still bound to their disks must be quite small, i.e., less than $2.4 \times 10^7\ M_\odot$.

We do not confirm the amount of H I previously reported in SQ. The total amount of H I detected by the VLA between 5597 and 6755 km s^{-1} is roughly $10^{10}\ M_\odot$, which is a factor of 2 lower than that reportedly detected by the WSRT. Most of this difference can be attributed to the integrated flux of the high-velocity cloud features. The discrepancy cannot be explained by significant differences in the instrumental performance of the two configurations and we suspect that it is related to the quality and processing of the WSRT data, which probably was compromised by low residual radar interference and unstable levels in the continuum emission. We are more confident in the VLA measurements because the data were free from these effects and the value of the integrated flux of the high-velocity gas is consistent with independent single-dish measurements obtained with smaller antennas.

The optical, X-ray, and radio continuum emission leaves little doubt that recent interactions have occurred in SQ. The radio continuum ridge visible in X-ray and Hα is the strongest evidence of a gaseous collision. But a collision between what two objects or components? NGC 7318B has been identified as the prime intruder and collision suspect, because it brings enough kinetic energy into the group to shock and ionize the gas. The continuum ridge in SQ, truly impressive in its scale, is about a factor of 4 larger than the radio bridge between the "Taffy" pair and exceeds the angular size of any of the bright galaxies in SQ. Given the large scale of the radio ridge, we favor the hypothesis that the H I tidal tail behind NGC 7320 originally filled the region connecting Arc-S and NW-HV and that a collision between NGC 7318B and this tidal tail fully ionized the H I intragroup gas now detectable as the Hα, X-ray, and radio continuum ridge. The intruder theory is attractive for three reasons: (1) there is a supply of faint H I–rich galaxies $\sim 15'$ from SQ's center; (2) the energy that the intruder deposits via interactions can be transformed into the thermal and nonthermal forms we observed in SQ; and (3) this source of energy can support the group against rapid (a few crossing times) collapse.

Unfortunately, there is no well-defined interaction scenario that can explain the H I tidal features in SQ, because none of the clouds are clearly linked with any of the bright galaxies. Some of the gas in Arc-N is at the end of a tidal tail that appears to emanate from NGC 7319, but the original source of H I in Arc-S is uncertain. The two NW features both strategically located near the tips of two tidal tails have systemic velocities very close to those of NGC 7318A/B and could be physically associated with their northern tails, as Plana et al. (1999) suggest. The SW feature is the only cloud that has a projected separation that is close to the one bright galaxy sharing a similar systemic velocity and this H I feature is found also at the end of a tidal tail/arm. Numerical simulations of Barnes & Hernquist (1992) have shown that large pools of gas can develop at the tip of tidal tails during a single encounter between two galaxies. When taken together, the conspicuous sites of the H I clouds in SQ are consistent with the predicted location of tidally liberated gas that has the potential to develop into dwarf galaxies. It is difficult to trace the culprit(s) involved in the interactions when the galaxies have undergone multiple scatterings as a result of their high number density. We must be cautious about inferences based on the results of numerical studies of interacting pairs when there are multiple interactions, because these interpretations are probably not completely valid in this case.

Intergalactic H I clouds with masses greater than $10^8\ M_\odot$ are extremely rare, as numerous null searches (Fisher & Tully 1981a; Lo & Sargent 1979) in nearby groups of galaxies have revealed, and yet SQ contains multiple cloud features clearly distinct from the disk of the luminous galaxies with no detectable levels of H I. Given the rarity of intergalactic H I clouds and the evidence of interactions (two large optical tidal tails, diffuse light surrounding the group, the radio continuum ridge, H I–deficient galaxies), a natural explanation for the H I is that its origin is tidal. The only other known group with as many cloud features as SQ is G11 (de Vaucouleurs et al. 1975) or GWa (Materne 1978), the nearby compact group that contains the Leo H I cloud complex. The general morphology of the two cloud complexes is similar in their relative dimensions, clumpiness, and ringlike shape. But unlike the intergalactic H I ring in Leo where there is no hint of diffuse stellar emission, the clouds in SQ are projected along the same directions as the blue and red diffuse stellar emission (Moles et al. 1998) that surrounds the entire group. In addition, the high-density regions of the H I are decorated with numerous Hα sources indicative of the current star-forming activity. There are some clumps of H I devoid of diffuse emission and Hα sources so that we cannot dismiss the possibility that some of the gas in SQ is primordial and remnants of the group formation process. The origin of the H I features in SQ still remains unresolved.

The authors gratefully acknowledge helpful discussions with A. del Olmo, C. Mendes de Oliveira, M. Moles, J. Perea, J. Sulentic, and C. Xu. We also thank Y. Ohyama for providing us with his published Hα image for comparisons and the referee for valuable comments. The data presented here were obtained using the VLA. The National Radio Astronomy Observatory is a facility of the National Science Foundation operated under cooperative agreement by the Associated Universities for Research in Astronomy, Inc.

REFERENCES

Allen, R. J. 1970, A&A, 7, 330
Allen, R. J., & Hartsuiker, J. W. 1972, Nature, 239, 324
Allen, R. J., & Sullivan, W. T., III. 1980, A&A, 84, 181
Arp, H. 1973, ApJ, 183, 411
Arp, H., & Lorre, J. 1976, ApJ, 210, 58
Balkowski, C., Bottinelli, L., Chamaraux, P., Gougenheim, L., & Heidmann, J. 1973, A&A, 25, 319
Barnes, J. E. 1996, in ASP Conf. 116, The Nature of Elliptical Galaxies, ed. M. Arnaboldi et al. (San Francisco: ASP), 469
Barnes, J. E., & Hernquist, L. 1992, Nature, 360, 715

Barnes, J. E., & Hernquist, L. 1996, ApJ, 471, 115
Brandt, J. C. 1960, ApJ, 131, 553
Burbidge, E. M., & Burbidge, G. R. 1961, ApJ, 134, 244
Burstein, D., & Heiles, C. 1978, ApJ, 225, 40
Condon, J. J., Helou, G., Sanders, D. B., & Soifer, B. T. 1993, AJ, 105, 1730
de Vaucouleurs, G. 1975, in Stars and Stellar Systems, Vol. IX, ed. A. Sandage, M. Sandage, & J. Kristen (Chicago: Univ. Chicago Press), 557
de Vaucouleurs, G., de Vaucouleurs, A., Corwin, H. G., Buta, R. J., Paturel, G., & Fouqué, P. 1991, Third Reference Catalogue of Bright Galaxies. (New York: Springer) (RC3)
Fisher, J. R., & Tully, R. B. 1981a, ApJ, 243, L23
———. 1981b, ApJS, 47, 139
Gao, Y., & Xu, C. 2000, ApJ, 542, L83
Gordon, K. J., & Gordon, C. P. 1979, Astrophys. Lett., 20, 9
Governato, F., Tozzi, P., & Cavaliere, A. 1996, ApJ, 458, 18
Harwit, M., Houck, J. R., Soifer, B. T., & Palumbo, G. G. C. 1987, ApJ, 315, 28
Hibbard, J. E., & Mihos, J. C. 1995, AJ, 110, 140
Hickson, P. 1982, ApJ, 255, 382
———. 1993, Astrophys. Lett., 29, 1
Hickson, P., Mendes de Oliveira, C., Huchra, J. P., & Palumbo, G. G. C. 1992, ApJ, 399, 353
Huchtmeier, W. K., & Richter, O.-G. 1988, A&A, 203, 237
Huchtmeier, W. K., Verdes-Montenegro, L., Yun, M. S., Del Olmo, A., & Perea, J. 2000, in IAU Colloq. 174, Small Galaxy Groups, ed. M. J. Valtonen & C. Flynn (ASP Conf. Ser. 209) (San Francisco: ASP), 154
Hunsberger, S. D., Charlton, J. C., & Zaritsky, D. 1996, ApJ, 462, 50
Kennicutt, R. C. 1998, ARA&A, 36, 189
Kenney, J. D. P., & Koopmann, R. A. 1999, AJ, 117, 181
Kenney, J. D. P., van Gorkom, J., & Vollmer, B. 2000, in ASP Conf. Ser. 240, Gas and Galaxy Evolution: A Celebration in Honor of the 20th Anniversary of the VLA, ed. J. Hibbard, M. Rupen & J. H. van Gorkom (San Francisco: ASP)
Lo, K. Y., & Sargent, W. L. W. 1979, ApJ, 227, 756
Materne, J. 1974, A&A, 35, 441
———. 1978, A&A, 63, 401
Moles, M., Marquez, I., & Sulentic, J. W. 1998, A&A, 334, 473
Moles, M., Sulentic, J. W., & Marquez, I. 1997, ApJ, 485, L69
Ohyama, Y., Nishiura, S., Murayama, T., & Taniguchi, Y. 1998, ApJ, 492, L25
Peterson, S. D., & Shostak, G. S. 1980, ApJ, 241, L1
Pietsch, W., Trinchieri, G., Arp, H., & Sulentic, J. W. 1997, A&A, 322, 89
Plana, H., Mendes de Oliveira, C., Amram, P., Bolte, M., Balkowski, C., & Boulesteix, J. 1999, ApJ, 516, L69
Roberts, M. S., & Haynes, M. P. 1994, ARA&A, 32, 115
Rood, H. J., & Williams, B. A. 1985, ApJ, 288, 535
Rupen, M. 1999, in ASP Conf. Ser. 180, Interferometric Imaging Workshop, ed. G. Taylor (San Francisco: ASP)
Sandage, A., & Tammann, G. A. 1981, A Revised Shapley-Ames Catalog of Bright Galaxies (Washington: Carnegie Inst. Washington)
Schneider, S. E. 1985, ApJ, 288, L33
Schneider, S. E., Skrutskie, M. F., Hacking, P. B., Young, J. S., & Dickman, R. L. 1989, AJ, 97, 666
Shostak, G. S. 1974, ApJ, 187, 19
Shostak, G. S., Sullivan, III, W. T., & Allen, R. J. 1984, A&A, 139, 15
Stephan, M. 1877, CR Acad. Sci. Paris, 84, 641
Sulentic, J. W. 1987, ApJ, 322, 605
———. 1997, ApJ, 482, 640
Sulentic, J. W., & Arp, H. 1983, AJ, 88, 267
Sulentic, J. W., Pietsch, W., & Arp, H. 1995, A&A, 298, 420
Sulentic, J. W., Rosado, M., Dultzin-Hacyan, D., Verdes-Montenegro, L., Trinchieri, G., Xu, C., & Pietsch, W. 2001, AJ, 122, 2993
Sullivan, W. T., III. 1980, A&A, 89, L3
Tammann, G. A. 1970, Astrophys. Lett., 7, 111
van der Hulst, J. M., & Rots, A. H. 1981, AJ, 86, 1775
Verdes-Montenegro, L., Yun, M. S., Williams, B. A., Huchtmeier, W. K., del Olmo, A., & Perea, J. 2000a, in IAU Colloq. 174, Small Galaxy Groups, ed. M. J. Valtonen & C. Flynn (ASP Conf. Ser. 209) (San Francisco: ASP), 154
———. 2000b, in ASP Conf. Ser. 240, Gas and Galaxy Evolution: A Celebration in Honor of the 20th Anniversary of the VLA, ed. J. Hibbard, M. Rupen & J. H. van Gorkom (San Francisco: ASP)
———. 2001, A&A, 377, 812
Vorontsov-Velyaminov, B. A. 1959, Atlas and Catalog of Interacting Galaxies (Moscow: Sternberg Inst.)
Williams, B. A., & Rood, H. J. 1987, ApJS, 63, 265
Williams, B. A., Van Gorkom, J. H., Yun, M. S., & Verdes-Montenegro, L. 1999, in Galaxy Interactions at Low and High Redshift, ed. J. E. Barnes, & D. B. Sanders (Dordrecht: Kluwer), 375
Williams, B. A., Yun, M. S. & Verdes-Montenegro, L. 1999, AAS Meeting, 194, 1905
Xu, C., Sulentic, J. W., & Tuffs, R. 1999, ApJ, 512, 178
Yun, M. S., Verdes-Montenegro, L., del Olmo, A., & Perea, J. 1997, ApJ, 475, L21
Zwicky, F. 1956, Ergeb. Exakten Naturwiss., 29, 344
Zwicky, F., & Kowal, C. T. 1968, Catalogue of Galaxies and Clusters of Galaxies, Vol. 6 (Pasadena: Caltech)